Neurobiology of Disease 34 (2009) 163–177

Contents lists available at ScienceDirect

Neurobiology of Disease

journal homepage: www.elsevier.com/locate/ynbdi

Inhibition of soluble TNF signaling in a mouse model of Alzheimer's disease prevents pre-plaque amyloid-associated neuropathology

Fiona E. McAlpine [a], Jae-Kyung Lee [a], Ashley S. Harms [a], Kelly A. Ruhn [a], Mathew Blurton-Jones [b], John Hong [a], Pritam Das [c], Todd E. Golde [c], Frank M. LaFerla [b], Salvatore Oddo [b], Armin Blesch [d], Malú G. Tansey [a,*]

[a] Department of Physiology, The University of Texas Southwestern Medical Center, 5323 Harry Hines Blvd., Dallas, TX 75390-9040, USA
[b] Department of Neurobiology and Behavior, University of California-Irvine, Irvine, CA 92697, USA
[c] Department of Neuroscience, Mayo Clinic, Jacksonville, FL 32224, USA
[d] Department of Neurosciences, University of California-San Diego, La Jolla, CA 92093, USA

ARTICLE INFO

Article history:
Received 29 December 2008
Accepted 9 January 2009
Available online 23 January 2009

Keywords:
Neuroinflammation
Alzheimer's disease
Tumor necrosis factor
3xTgAD
Amyloid-β
Amyloid precursor protein
β-CTF
Lentivirus

ABSTRACT

Microglial activation and overproduction of inflammatory mediators in the central nervous system (CNS) have been implicated in Alzheimer's disease (AD). Elevated levels of the pro-inflammatory cytokine tumor necrosis factor (TNF) have been reported in serum and post-mortem brains of patients with AD, but its role in progression of AD is unclear. Using novel engineered dominant negative TNF inhibitors (DN-TNFs) selective for soluble TNF (solTNF), we investigated whether blocking TNF signaling with chronic infusion of the recombinant DN-TNF XENP345 or a single injection of a lentivirus encoding DN-TNF prevented the acceleration of AD-like pathology induced by chronic systemic inflammation in 3xTgAD mice. We found that chronic inhibition of solTNF signaling with either approach decreased the LPS-induced accumulation of 6E10-immunoreactive protein in hippocampus, cortex, and amygdala. Immunohistological and biochemical approaches using a C-terminal APP antibody indicated that a major fraction of the accumulated protein was likely to be C-terminal APP fragments (β-CTF) while a minor fraction consisted of Aβ40 and 42. Genetic inactivation of TNFR1-mediated TNF signaling in 3xTgAD mice yielded similar results. Taken together, our studies indicate that soluble TNF is a critical mediator of the effects of neuroinflammation on early (pre-plaque) pathology in 3xTgAD mice. Targeted inhibition of solTNF in the CNS may slow the appearance of amyloid-associated pathology, cognitive deficits, and potentially the progressive loss of neurons in AD.

Introduction

Although the etiology of idiopathic Alzheimer's disease (AD) in humans is unknown, mutations in amyloid precursor protein (APP) or presenilin-1, a component of the γ-secretase complex, result in overproduction of Aβ40 and 42 peptides and are sufficient to cause disease (Cai et al., 1993; Citron et al., 1992; Goate et al., 1991; Lemere et al., 1996; Lopera et al., 1997; Nee et al., 1983; Whalen et al., 2005). Cleavage of APP by α- and β-secretases also results in the retention of intracellular fragments which can be further cleaved by γ-secretase. Specifically, cleavage by α-secretase results in an 83 amino acid fragment, known as C83 or α-C-terminal fragment (α-CTF (Estus et al., 1992) which is further processed by γ-secretase to produce the non-amyloidogenic fragment p3 (Haass et al., 1993). Cleavage of APP by β-secretase produces a 99 amino acid fragment known as C99 or β-CTF (Sinha and Lieberburg, 1999) which is further cleaved by γ-secretase to produce Aβ peptides. β-CTF alters ionic homeostasis (Fraser et al., 1997) and exerts neurotoxicity in differentiated PC12 cells (Yankner et al., 1989) and in transgenic mice (Oster-Granite et al., 1996). Neuronal cells bearing familial AD (FAD) mutations accumulate β-CTF intracellularly (McPhie et al., 1997), implicating its involvement in AD pathogenesis.

Experimental and clinical evidence suggests a close association between neuroinflammation and AD pathogenesis (Akiyama et al., 2000). Overproduction of inflammatory mediators in the brain occurs when microglia, which are often found in close physical association with amyloid plaques in AD brains, become chronically activated. It has been proposed that elevated levels of pro-inflammatory cytokines, including tumor necrosis factor (TNF), may inhibit phagocytosis of Aβ in AD brains thereby hindering efficient plaque removal by resident microglia (Koenigsknecht-Talboo and Landreth, 2005). Clinically, TNF-driven processes have been strongly implicated in AD pathology and may contribute to cognitive dysfunction and accelerated progression of AD (Alvarez et al., 2007; Collins et al., 2000; Fillit et al., 1991; Ma et al., 2004; Paganelli et al., 2002; Tan et al., 2007; Tobinick et al., 2006).

* Corresponding author. Fax: +1 214 645 6049.
E-mail address: malu.tansey@utsouthwestern.edu (M.G. Tansey).
Available online on ScienceDirect (www.sciencedirect.com).

0969-9961/$ – see front matter © 2009 Elsevier Inc. All rights reserved.
doi:10.1016/j.nbd.2009.01.006

In support of the idea that chronic systemic inflammatory disease may accelerate AD pathogenesis, the bacterial endotoxin lipopolysaccharide (LPS), a potent trigger of inflammation that elicits production of TNF and other cytokines (Flick and Gifford, 1986), can accelerate the appearance and severity of AD pathology in several animal models of AD. These include the APPV717F mouse (Qiao et al., 2001), the APPSwe Tg2576 mouse (Sheng et al., 2003), and the 3xTgAD mouse (Kitazawa et al., 2005) in which up-regulation of TNF mRNA precedes the appearance of amyloid-associated pathology (Janelsins et al., 2005) and correlates with cognitive deficits (Billings et al., 2005). Taken together, these observations provide compelling rationale to investigate new therapeutic approaches that selectively target the TNF pathway in pre-clinical models of AD. The main goal of our studies was to investigate the feasibility and efficacy of novel anti-TNF therapeutics in blocking early development of amyloid-associated pathology in 3xTgAD mice (Oddo et al., 2003a,b) exposed to chronic peripheral inflammation.

Materials and methods

Reagents and materials

Unless otherwise stated, all chemical and tissue culture reagents were obtained from Sigma-Aldrich Corp (St. Louis, MO). Tissue culture plastic was obtained from Corning (Corning, NY). Recombinant mouse TNF was obtained from R&D Systems (Minneapolis, MN). The dominant negative XENP345 was provided by Xencor, Inc.; DN-TNF neutralizes solTNF signaling by forming dominant negative heterotrimers that have significantly attenuated binding affinity for TNF receptors (Steed et al., 2003; Zalevsky et al., 2007) thereby lowering the effective concentration of solTNF without affecting overall production levels of TNF or the biological activity of transmembrane TNF (tmTNF), including its role in maintaining innate immunity (Zalevsky et al., 2007).

Animal studies

3xTgAD mice are of a mixed 129/C57BL6 genetic background (Oddo et al., 2003b) and were generated by Dr. Frank M. LaFerla (University of California at Irvine). TNFR1-deficient mice on a C57BL6 genetic background were obtained from Jackson Laboratories (Bar Harbor, ME). Animals were housed in pathogen-free, climate-controlled facilities and allowed to have food and water *ad libitum* at the Animal Resources Center at The University of Texas Southwestern Medical Center. All animal studies were approved by the Institutional Animal Care and Use Committee at The University of Texas Southwestern Medical Center at Dallas.

Intrahippocampal infusion of XENP 345 and systemic LPS injections

Young adult (4.5 month old) 3xTgAD mice were anesthetized continuously with 2.5% halothane (Halocarbon Laboratories, River Edge, NJ) and placed in a stereotaxic frame (David Kopf Instruments, Tujunga, CA). We inserted a cannula (gauge 28; Plastics One, Roanoke, VA) connected via polyethylene tubing to a subcutaneously implanted osmotic minipump (model 2004, Alzet, Cupertino, CA) preloaded with vehicle (sterile PBS with 10% glycerol) or the treatment agent XENP345 (0.1 mg/kg/day) at the coordinates for hippocampus CA1 in the right hemisphere (anterioposterior (AP): −2.0 mm from bregma, mediolateral (ML): −2.0 mm and dorsoventral (DV): −1.6 mm below dura), per the mouse brain atlas (Paxinos and Franklin, 2001). The recombinant dominant-negative human TNF variant XENP345 (Steed et al., 2003; Zalevsky et al., 2007) was bacterially produced and formulated by Xencor, Inc. (Monrovia, CA) to contain <0.1 endotoxin units (E.U.)/mg. Cannulae were secured to the skull with surgical glue and left in position for 4 weeks. The mice were injected with either 0.25 mg/kg (7.5×10^5 endotoxin units (E.U.)/kg LPS (from *Escherichia coli* O111:B4; 3.0×10^6 E.U./mg, Sigma-Aldrich Corp., St. Louis, MO) or an equivalent volume of sterile saline (B. Braun Medical Inc., Bethlehem, PA). intraperitoneally (i.p.) twice weekly for 4 weeks.

Cloning of DN-TNF sequences into lentiviral vector

The human pro-DN-TNF sequence, provided to us by David E. Szymkowski (Xencor, Inc., Monrovia, CA), included a signal peptide sequence and was that of the TNF variant A145R/I97T. The DN-TNF sequence was subcloned into a constitutive self-inactivating lentiviral vector based on the plasmid pLV (Pfeifer et al., 2002) 5′ of an internal ribosome entry site (IRES) followed by the GFP coding sequence. The GFP expressing lentiviral plasmid has been described previously (Pfeifer et al., 2002; Taylor et al., 2006). DN-TNF or GFP expression was driven by the CMV enhancer/chicken β-actin hybrid promoter (CAG).

Preparation and purification of lentivirus stocks

Lentivirus stocks were produced and purified according to a previously published protocol (Taylor et al., 2006). The final titer was 125 μg/mL p24 and 1.6×10^9 infectious units/mL for the negative control lentivirus-GFP and 980 μg/mL p24 and 8×10^8 IU/mL for lentivirus-DN-TNF.

Measurement of DN-TNF protein by quantitative human TNF ELISA

Neuro2a cells were infected with 10 M.O.I. lentivirus-DN-TNF. Media was collected and replaced every 24 h up to 72 h post-infection. The DN-TNF produced by the cells was measured by quantitative ELISA specific for human TNF and non-crossreactive with mouse TNF (Biosource/Invitrogen, Carlsbad, CA).

Stereotaxic surgeries for lentivirus injections

Young adult (3 month-old) 3xTgAD mice were anesthetized continuously with 2.5% halothane and placed in a stereotaxic frame. A 30 gauge needle (Hamilton Company, Reno, NV) was inserted to reach the coordinates for the 3rd ventricle (AP: −0.82 mm from bregma, ML: −0.47 mm from midline, DV: −2.5 mm from dura) per the mouse brain atlas (Paxinos and Franklin, 2001). Due to the risk of damaging blood vessels by injecting so close to midline, we used an angled approach to reach the coordinates above (12° angle, AP: −0.82 from bregma, ML: −1.0 mm from midline, DV: −2.55 mm from dura). An injection of 1 μL of lenti-DN-TNF or lenti-GFP at 100 μg p24/mL was administered via an automated injector (Stoelting Co., Wood Dale, IL) using a 5 μL Hamilton microsyringe. Mice were allowed to express the lentivirus for 6 weeks and were then injected with 0.25 mg/kg (7.5×10^5 E.U./kg) LPS i.p. twice weekly for 6 weeks.

Primary microglial cultures from 3xTgAD mice

Primary microglial cells were isolated from postnatal day 1 (P1) 3xTgAD mouse pups and cultured as previously described (Saura et al., 2003). Quantification of activated microglia was performed by counting the number of primary microglia which stained brightly positive for CD45 in 10 fields per well in 3 separate wells for each treatment condition. Total number of microglia was quantified by counting all cells stained positive for CD45 (strongly and weakly); these counts matched the total number of nuclei counterstained with Hoechst 33258).

Astrocyte cell line culture

The murine astrocyte cell line SS01 (a gift from Dr. Robert Bachoo, University of Texas Southwestern Medical Center, Dallas, TX) was maintained in DMEM supplemented with 10% heat-inactivated FBS.

Fluorescence immunohistochemistry/immunocytochemistry

Immunohistochemistry was performed on brain sections as previously described (McCoy et al., 2006). 10 μm cryosections were incubated with mouse anti-human Aβ clone 6E10 (Chemicon, Temecula, CA, 1:3000). Immunoreactivity was visualized using an Alexa fluor-conjugated secondary antibody, goat anti-mouse 488 (Molecular Probes/Invitrogen, Carlsbad, CA, 1:1000). Sections were counterstained with the nuclear dye Hoechst 33258 (bisbenzimide, 1:20,000). Immunocytochemistry was performed as previously described (McCoy et al., 2006). Cells were incubated with rabbit anti-NFκB p65 RelA (Santa Cruz Biotechnology, Santa Cruz, CA, 1:200) or rat-anti-CD45 to visualize microglia (Serotec, 1:500). Immunoreactivity was visualized using Alexa fluor-conjugated secondary antibodies (goat anti-rabbit 594 or goat anti-rat 594, 1:1000) followed by nuclear counterstain as above.

Brightfield immunohistochemistry/immunocytochemistry

Brain sections on slides were stained using a previously published protocol (Frank et al., 2003). Epitope unmasking required for anti-Aβ (6E10), anti-APP (C9), Aβ40- or 42-specific, and N-terminal APP staining consisted of a brief incubation in 88% formic acid (Fisher Scientific, Fair Lawn, NJ). 30 μm cryosections were incubated with mouse anti-human Aβ clone 6E10 (1:1000), rabbit anti-human Aβ40 (Chemicon, 1:100), mouse anti-Aβ40 (Mab 13.1.1, 1:500, (Das et al., 2003; Kim et al., 2007), rabbit anti-human Aβ42 (Invitrogen, 1:100), mouse anti-Aβ42 (Mab 2.1.3, 1:500, (Das et al., 2003; Kim et al., 2007), rabbit anti-APP (C9, 1:500, (Kimberly et al., 2005), chicken anti-GFP (Chemicon, 1:500), rat anti-mouse CD68 (Serotec, 1:500), or rat anti-mouse CD45 (Serotec, 1:500), mouse anti-APP (22C11, 1:100, Chemicon). Sections were then incubated with biotinylated secondary antibodies (horse anti-mouse, goat anti-rabbit, goat anti-chicken, or rabbit anti-goat, Vector Laboratories, Burlingame, CA, 1:1000) followed by incubation with neutravidin-HRP (Pierce Biotechnology, Rockford, IL). Immunoreactivity was visualized by reaction with diaminobenzidine (DAB) with nickel sulfate (to produce a purple-blue reaction product) or without ammonium nickel sulfate (to produce a brown reaction product).

Immunofluorescence confocal microscopy

6-month old 3xTg-AD mice were sacrificed by Euthasol overdose and cardiac perfusion with 0.01 M phosphate buffered saline (PBS). Brains were rapidly removed, postfixed in 4% paraformaldehyde (pH-7.4) for 48 h, and cut as 50 μm thick coronal sections using a Vibratome. To examine intraneuronal Aβ, sections were double-labeled with the monoclonal antibody 6E10 (Covance, Emeryville CA) and a polyclonal antibody directed against the C-terminus of amyloid precursor protein (APP) (Invitrogen). Primary antibodies were applied overnight at 4 °C and following rinses were detected with anti-mouse Alexa 555 (Invitrogen, 1:200, red) and anti-rabbit Alexa 488 (Invitrogen, 1:200, green). After rinsing, sections were mounted on slides and coverslipped using Fluoromount-G (Southern Biotech). Specificity of all primary antibodies was confirmed by Western blot and also by omission of primary antibody which demonstrated no staining (data not shown). 6E10 recognizes amino acids 1–16 within the Aβ sequence and thus can also recognize full-length APP or the β-CTF of APP. Double-label confocal microscopy was therefore utilized to identify interneuronal Aβ (red only) versus full-length APP or β-CTF immunoreactivity (overlap of red and green), or α-CTF (green only). Immunofluorescent sections were visualized using a Bio-Rad 2100 confocal imaging system equipped with Argon, HeNe, and Red Diode lasers (Bio-Rad Laboratories, Hercules, CA). To avoid non-specific bleed-through, each laser line was excited and detected independently using lambda-strobing mode. All images represent either single confocal Z-slices or Z-stacks. Kruskal–Wallis analysis was performed to assess significance between experimental conditions.

Stereological analyses

Stereological analyses to estimate the number of amyloid-positive cells were performed using the optical fractionator module of Stereoinvestigator software (MicroBrightField, Williston, VT). Contours were traced around the hippocampus, cortex, and amygdala under the magnification of a 2× objective as delineated by the mouse brain atlas (Paxinos and Franklin, 2001). Aβ positive (immunoreactive for 6E10) cells were counted under a 60× oil immersion objective using random and systematic counting frames (size: 50 μm×50 μm) with an 18 um optical dissector, 2 μm upper and lower guard zones in a 430 μm×280 μm grid. All reported values had a Gundersen coefficient of error (CE) values of less than 0.10.

Biochemical analysis of Aβ40 and 42

Aβ peptides from mouse brains were extracted and measured as previously described (Levites et al., 2006). Briefly, each frozen hemi brain was sequentially extracted in a two-step extraction involving, extraction in RIPA buffer followed by 70% formic acid. The following antibodies against Abeta were used in a sandwich capture ELISA for measuring Aβ levels as described before (Levites et al., 2006). For brain Aβ40, Ab9 (Aβ1–16) was used for capture and Ab40.1-HRP for detection. For brain Aβ42, Ab42.2 was used for capture and Ab9-HRP for detection.

Immunoblot analyses

Flash-frozen mouse hemispheres were homogenized in ice-cold RIPA buffer with protease inhibitor cocktail (Roche, Indianapolis, IN). Protein samples were diluted in 2× Laemmli sample buffer (62.5 mM Tris–HCl, pH 6.8, 20% glycerol, 2% SDS, 0.1% bromophenol blue, 5% 2-mercaptoethanol), boiled for 5 min, and run on a 4–20% Tris–Glycine gel (for PS1 and BACE1) or a 10–20% gel (APP and CTFs) for 90 min at 125 V in 1× Tris–Glycine–SDS running buffer or 90 min at 130 V in 1× Tricine–SDS running buffer. The gels were transferred onto a 0.2 μm nitrocellulose membrane (Biorad) at 30 V for 1 h 30 min. The membranes were blocked in 5% milk in TBST (1× TBS with 0.1% Tween-20) for 1 h and incubated in primary antibodies (anti-APP C9, 1:500; anti-PS1, 1:2500; anti-BACE1, 1:1000; anti-alpha-tubulin, 1:5000) overnight at 4 °C. The membranes were then washed three times 10 min in TBST, incubated in secondary antibodies (goat-anti-mouse-HRP, 1:2500, or goat-anti-rabbit-HRP, 1:5000) for 1 h at room temperature, then washed five times 10 min in TBST. The membrane was then incubated for 1 min at room temperature in WestDura chemiluminescent substrate (Thermo Scientific, Rockford, IL) and imaged using the ChemiImager 5500 (Alpha Innotech, San Leandro, CA).

Real-time quantitative PCR

Quantitative real-time PCR was performed as previously described (Valasek and Repa, 2005). Briefly, hippocampi were isolated from 3xTgAD mice given chronic systemic i.p. injections of saline or low-dose (7.5×10^5 E.U./kg) LPS for 6 weeks. RNA was extracted using Tri-Reagent (Molecular Research Center, Inc., Cincinnati, OH), treated with DNAse I (Invitrogen), and reverse transcribed using Superscript II RNAse H-reverse transcriptase (Invitrogen). Quantitative real-time PCR was performed using an ABI Prism 7900HT Fast Detection System (Applied Biosystems, Forster City, CA). Each reaction was performed in a volume of 20 μL that contained 50 ng cDNA, 10 μL SYBR Green PCR Master Mix (Applied Biosystems), and 150 nM of each (forward and reverse) PCR primer. All reactions were performed in triplicate. Levels of the various

mRNAs were normalized to those of the mouse housekeeping gene cyclophilin. The following forward and reverse primers were used:

mCyclophilin forward:	5′-TGGAGAGCACCAAGACAGACA-3′
mCyclophilin reverse:	5′-TGCCGGAGTCGACAATGAT-3′
mAPP forward:	5′-GTGCCAGCCAATACCGAAAA-5′
mAPP reverse:	5′-TTGGATGTTTGTCAGCCCAGAA-3′
mBACE1 forward:	5′-CAATCAGTCCTTCCGCATCA-3′
mBACE1 reverse:	5′-TGTGAGACAGCGAACTTGTAACAG-3′
mApoE forward:	5′-GCAGGCGGAGATCTTCCA-3′
mApoE reverse:	5′-CCACTGGCGATGCATGTC-3′
hAPP forward:	5′-CCGCTCTGCAGGCTGTTC-3′
hAPP reverse:	5′-CGCGGACATACTTCTTTAGCATATT-3′

Statistical analysis

The differences between means of stereological estimates of Aβ positive cells in lentivirus-infected animals and between means of nuclear counts within the hilus and amyloid beta-positive cells were subjected to a one-tailed Student's *t*-test. The differences between means of stereological estimates of 6E10-positive cells in the hippocampus of animals that received XENP 345 infusion via indwelling cannulae were subjected to a one-way ANOVA followed by Tukey's test for post-hoc analysis. Differences between means of stereological estimates of 6E10-positive cells in cortex, hippocampus and amygdala were subjected to a one-tailed *t*-test. Differences in numbers of activated primary microglia were subjected to a one-way ANOVA followed by Tukey's post-hoc test. Differences in Aβ40 and Aβ42 levels were subjected to one-factor ANOVA. For immunofluorescence confocal microscopy, Kruskal–Wallis analysis was performed to assess significance between experimental conditions. Values expressed are the means ± S.E.M., * denotes $p<0.05$.

Results

Intrahippocampal infusion of XENP345 prevents accumulation of 6E10-immunoreactivity induced by chronic systemic inflammation

3xTgAD mice display age-dependent AD-like pathology in the hippocampus and entorhinal cortex which can be accelerated by chronic systemic inflammation induced by bacterial endotoxin lipopolysaccharide (LPS), a potent trigger of inflammation that elicits production of TNF and other cytokines (Flick and Gifford, 1986). In order to investigate the extent to which soluble TNF mediates the LPS-induced accumulation of 6E10-immunoreactive protein reported in 3xTgAD mice (Kitazawa et al., 2005), we fitted 4.5 month old mice with osmotic pumps to administer 0.1 mg/kg/day of the DN-TNF variant XENP345 or an equivalent volume of vehicle into the hippocampus for 28 days. Our experimental design consisted of placing a cannula in the CA1 region of the hippocampus in the right hemisphere of the brain and, concurrent with the XENP345 or saline infusion, administering 0.25 mg/kg LPS (7.5×10^5 E.U./kg) intraperitoneally (i.p.) twice a week for one month (Fig. 1A). The hippocampus was chosen as a brain region of interest based on the report that 3xTgAD mice display AD-like pathology in the hippocampus by 6 months of age (Oddo et al., 2003a). Moreover, we chose the chronic systemic low-dose LPS regimen because it has been shown to accelerate the appearance of AD-like pathology in several other mouse models of AD (Kitazawa et al., 2005; Qiao et al., 2001; Sheng et al., 2003). Immunohistological analysis of brain sections from 3xTgAD animals fitted with pumps dispensing XENP345 and exposed to chronic systemic inflammation showed a marked qualitative reduction in neurons accumulating 6E10-immunoreactive material in the hilus compared to animals fitted with pumps dispensing saline and exposed to chronic systemic inflammation (Fig. 1B). Non-transgenic mice of the same genetic background did not display accumulation of 6E10-IR protein in response to chronic systemic inflammation in hippocampus (Fig. 1B) or any other brain region. Counts in the hilar region of the hippocampus revealed that administration of XENP345 significantly reduced the appearance of 6E10-IR protein in the hilus of the LPS-treated 3xTgAD mice compared to the saline-infused animals ($p<0.05$ by one-tailed Student's *t*-test) (Fig. 1C). This effect was also observed in parietal, temporal and entorhinal cortex as well as amygdala of LPS-treated mice (data not shown). Of note, the XENP345 treatment did not result in a reduction in the number of total cells (as measured by bisbenzimide-positive nuclei) in the regions where reduction in 6E10-IR was observed (Fig. 1D). To rule out the possibility that increased expression of 6E10-immunoreactive protein was a result of increased transcription of the human APP transgene, we performed real-time quantitative PCR analyses on freshly dissected hippocampal tissue to measure mRNA levels of the human APP transgene as well as mouse APP, BACE1 and ApoE. In agreement with previous findings (Kitazawa et al., 2005), we found that the chronic systemic inflammation regimen did not induce robust changes in expression of the transgene or the aforementioned murine genes (Supplementary Fig. S1). In a second experimental paradigm, 4.5 month old 3xTgAD mice were fitted with osmotic pumps for delivery of either saline or XENP345 for 1 month. During this time, the mice were injected i.p. twice a week with either 7.5×10^5 E.U./kg of LPS or an equivalent volume of saline (Fig. 2A). The brains of these mice were stained with the 6E10 antibody and subjected to stereological counts of 6E10-positive cells throughout the hippocampus ipsilateral and contralateral to the cannula. A gross comparison of brain regions stained with 6E10 revealed a qualitative increase in the extent of intraneuronal accumulation of 6E10-IR species in the total hippocampus (Fig. 2B) and specifically the hippocampal CA1 region (Fig. 2C) of animals infused with saline and exposed to chronic systemic LPS which did not occur in animals infused with XENP345 in the hippocampus and exposed to chronic systemic inflammation. Quantitative stereological analysis revealed that intrahippocampal administration of XENP345 inhibited the appearance of 6E10-positive cells ($p<0.05$ by one-way ANOVA and Tukey's post-hoc test) in LPS-injected mice (Fig. 2D) on both ipsilateral and contralateral hemispheres, possibly due to circulation of the inhibitor to the contralateral side. On the basis of these results we concluded that short term inhibition of solTNF in the hippocampus of young adult 3xTgAD mice blocks the accumulation of a 6E10-IR amyloid-associated protein(s) induced by chronic systemic inflammation.

Design and in vitro validation of lentiviral DN-TNF activity

Although chronic infusion of DN-TNF enabled us to block soluble TNF signaling in the hippocampus for a period of one month, a different approach was needed to obtain longer term inhibition of TNF activity and reach other parts of the brain affected by amyloid accumulation, such as the entorhinal cortex. To achieve this end, we chose to use a lentivirus-based approach because lentivirii infect non-mitotic cells and because expression of the desired gene can be maintained for periods of at least one year (Blomer et al., 1997). The sequence of the human TNF variant A145R/I97T (Steed et al., 2003), including the TACE cleavage site that converts the transmembrane form of the protein into a soluble form (Aggarwal et al., 2000), was subcloned into a self-inactivating lentiviral vector downstream from the CMV enhancer/chicken β-actin (CAG) promoter (Supplementary Fig. S2A). The lentiviral vector also contains an IRES-driven green fluorescence protein (GFP) sequence which allowed us to monitor *in vitro* and *in vivo* expression using endogenous GFP fluorescence or anti-GFP immunohistochemistry. The control vector consisted of the GFP sequence driven by the CAG promoter.

To establish that transduction of cells with lenti-DN-TNF resulted in production of measurable DN-TNF protein, the level of DN-TNF production in the conditioned media of cells transduced with the lentivirus was measured using a quantitative human TNF ELISA to

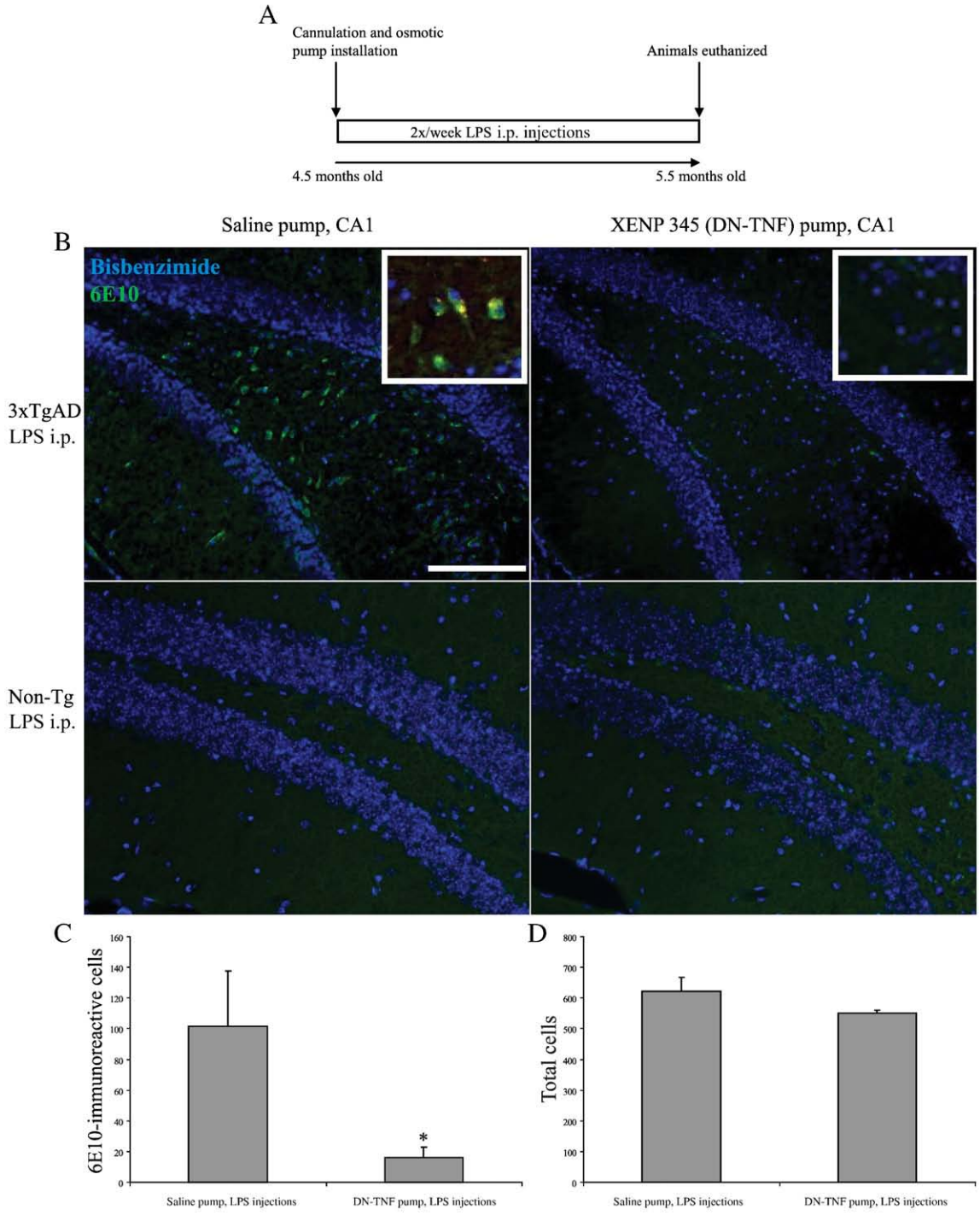

Fig. 1. Hippocampal infusion of XENP345 attenuates appearance of intraneuronal 6E10-immunoreactive protein induced by chronic systemic inflammation in 3xTgAD mice. (A) Schematic of experimental design: 4.5 month old mice were cannulated in the CA1 region of the hippocampus in the right hemisphere of the brain and fitted with osmotic pumps that delivered 0.1 mg/kg/day XENP345 or an equivalent volume of vehicle for 4 weeks. During these 4 weeks, animals were given 7.5×10^5 E.U./kg of LPS twice a week. (B) Immunohistological analysis of 6E10 immunoreactivity in hippocampal brain sections reveals that 3xTgAD mice that received intrahippocampal saline and i.p. LPS displayed significant accumulation of intraneuronal 6E10-imunoreactive protein (green). Inset shows 6E10-positive neurons in the hilus, magnified. 3xTgAD mice that received intrahippocampal XENP345 and i.p. LPS displayed reduced intraneuronal 6E10-immunoreactivity compared to those that received intrahippocampal saline and i.p. LPS. Inset shows 6E10-negative neurons in the hilus, magnified. Non-Tg animals of the same genetic background that received intrahippocampal saline or XENP345 and i.p. LPS displayed no intraneuronal 6E10-immunoreactive protein. Nuclei in (B) are counterstained with bisbenzimide (blue). Scale bar = 200 μm. (C) Quantification of 6E10-positive neurons in brain sections from animals that received intrahippocampal saline/LPS i.p. or intrahippocampal XENP345/LPS i.p. reveals a statistically significant difference in 6E10-immunoreactive protein accumulation between 3xTgAD saline/LPS and 3xTgAD XENP345/LPS groups. Values shown are group means ± SEM for $n=4$ animals per group, * denotes $p<0.05$ by one-tailed Student's t-test. (D) Quantification of total cells (nuclei counterstained with bisbenzimide) in the hilus of 3xTgAD animals infused with intrahippocampal XENP345 or saline reveals no significant difference between groups by one-tailed Student's t-test, confirming that reduction in Aβ is not due to loss of a TNF-dependent subpopulation of cells in the hilus. Values shown are group means ± SEM for $n=4$ animals per group.

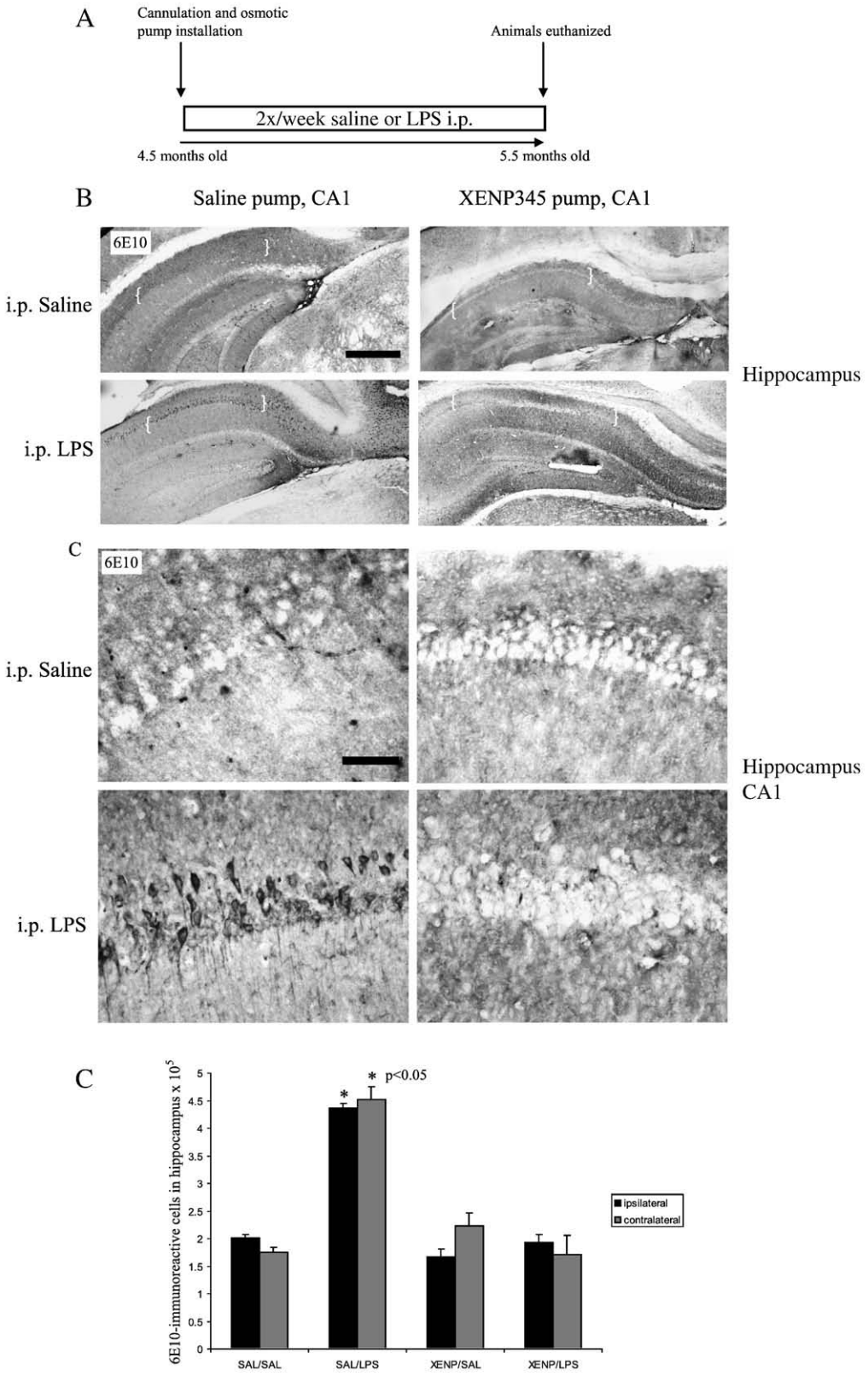

Fig. 2. Hippocampal infusion of XENP345 reduces appearance of intraneuronal 6E10-immunoreactive protein. (A) Schematic of experimental design: 4.5 month old mice were cannulated in the CA1 region of the hippocampus in the right hemisphere of the brain and fitted with osmotic pumps that delivered 0.1 mg/kg/day XENP345 or an equivalent volume of vehicle for 4 weeks. During these 4 weeks, animals were given 7.5×10^5 E.U./kg of LPS or an equivalent volume of saline twice a week. (B, C) Animals that were injected with i.p. low-dose LPS show increased 6E10-immunoreactive protein in the hippocampus; this increase is inhibited by XENP345. (A) Images were taken at 4× magnification. CA1 is surrounded by curly brackets, scale bar = 500 μm. (B) Images were taken at 40× magnification, scale bar = 50 μm. (D) Stereological analysis of 6E10-positive cell number in the hippocampus ipsilateral and contralateral to the cannula in 3xTgAD mice that received intrahippocampal saline or XENP345 and i.p. saline or LPS. Values shown are group means ± SEM for $n = 4$ animals per group. * denotes significantly different from saline pump/saline injections at $p < 0.05$) by one-way ANOVA followed by Tukey's post-hoc test.

specifically detect the human DN-TNF protein. The DN-TNF protein is not detected by ELISA specific for mouse TNF, nor is mouse TNF detected by ELISA specific for human TNF (data not shown). We found that Neuro2a murine neuroblastoma cells infected with lenti-DN-TNF produced daily amounts of DN-TNF into the conditioned media in the 10 ng/mL range over the 3-day time course assayed (Supplementary Fig. S2B), an amount that should be sufficient to neutralize up to 10 ng/mL solTNF *in vitro* (Steed et al., 2003; Zalevsky et al., 2007). To confirm that the lentiviral-derived DN-TNF was biologically active, we used several different *in vitro* functional assays. First, we assessed TNF pathway activation status by measuring cytoplasmic-to-nuclear translocation of the NFκB subunit p65 RelA (Hohmann et al., 1990) immunocytochemically in a murine astrocyte cell line. NFκB translocation in response to 2 ng/mL TNF was detectable in mock-transduced and lenti-GFP-transduced cells (Fig. 3A). In contrast, transduction with lenti-DN-TNF blocked TNF-induced cytoplasmic-to nuclear translocation of the p65 subunit of NFkB (Fig. 3A), indicating that transduction of cells with a lentivirus encoding DN-TNF resulted in proper expression of functionally active protein capable of antagonizing solTNF signaling. Next, we investigated the extent to which primary microglia transduced with lenti-DN-TNF responded to a TNF challenge. Primary microglial cultures from 3xTgAD mice were transduced with lenti-DN-TNF, lenti-GFP, or mock-transduced. We quantified microglial activation in response to 10 ng/mL TNF using immunocytochemistry for the microglial activation marker CD45. We used CD45 as a pan-microglia marker, as it stained all microglia in the dish, and used its upregulation especially in the nucleus as a measure of activation. The numbers of CD45-positive cells in each treatment group were used to normalize the numbers of activated microglia. Mock- and lenti-GFP transduced microglia responded to TNF treatment by upregulating CD45 expression (Fig. 3B). Mock-transduced cells, cells transduced with lenti-DN-TNF, or cells transduced with the negative control lenti-GFP were challenged with 10 ng/mL solTNF in the presence of excess dominant negative TNF protein inhibitor XENP345 (200 ng/mL) as a positive control for suppression of TNF signaling. Cultures that were mock-transduced or transduced with lenti-GFP displayed a significant increase in the percent of activated microglia in response to solTNF treatment, whereas lenti-DN-TNF-transduced cells displayed baseline levels of microglia activation, equivalent to the reduction in signaling achieved using XENP345 (Fig. 3C). On the basis of these studies, we hypothesized that transduction of mouse brains with lenti-DN-TNF should also result in functional antagonism of TNF-dependent processes *in vivo*.

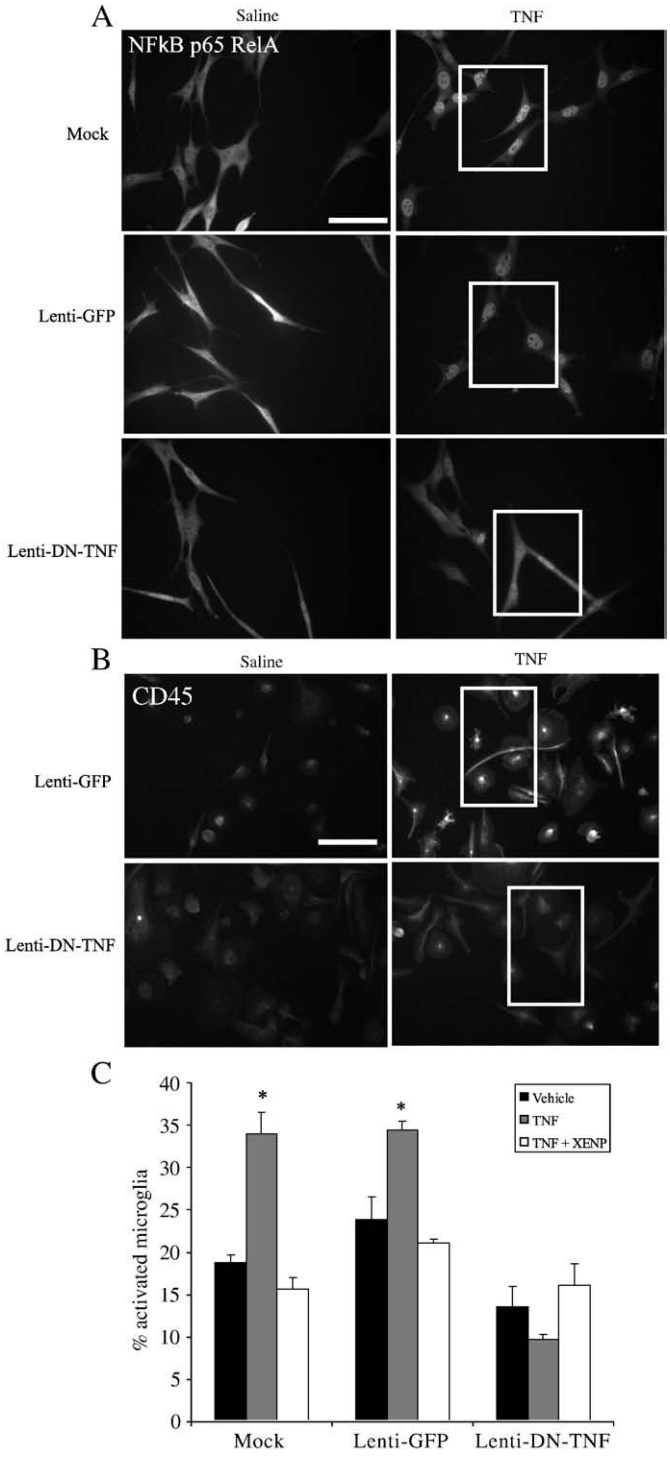

Lenti-DN-TNF prevents accumulation of intraneuronal 6E10-immunoreactivity in young 3xTgAD mice exposed to chronic systemic inflammation

To investigate the extent to which lentiviral-derived DN-TNF could block the LPS-induced accumulation of intraneuronal amyloid-related species accumulation, we selected 3 month-old 3xTgAD mice to coincide with the time of TNF mRNA upregulation (Janelsins et al., 2005) and the earliest appearance of intraneuronal 6E10-immunoreactive protein in the entorhinal cortex (Oddo et al., 2003a). Intracerebroventricular (ICV) injections of lenti-DN-TNF or lenti-GFP

Fig. 3. *In vitro* validation of the biological activity of lentiviral-derived DN-TNF in primary glial cells. (A) Transduction of SS01 murine astrocytes blocks TNF-induced NFκB pathway activation as measured by cytoplasmic-to-nuclear enrichment of the p65RelA subunit. SS01 cells were mock-transduced or transduced with lenti-GFP or lenti-DN-TNF 24 h after plating. Forty-eight hours later, cells were stimulated with saline vehicle (left panels) or 2 ng/mL TNF (right panels) for 15 min. Cells were fixed and immunostained with an antibody specific to the p65RelA subunit of NFκB. All cells display detectable cytoplasmic localization of p65 prior to stimulation. Upon stimulation with TNF, mock- and lenti-GFP-transduced cells display enhanced nuclear localization of p65 (white box), whereas lenti-DN-TNF-transduced cells still display a high degree of cytoplasmic p65 staining (white box). Scale bar = 50 μm. (B, C) Transduction of primary microglia with lenti-DN-TNF blocks TNF-induced microglia activation. Primary microglia cultures from 3xTgAD mice were mock-transduced or transduced with lenti-DN-TNF, or lenti-GFP. After 48 h, cells were treated with saline vehicle, 10 ng/mL TNF alone or 10 ng/mL TNF + 200 ng/mL XENP345 as a positive control for TNF inhibition. Cells were fixed 24 h later and immunostained with the microglial activation marker CD45. (B) Images of primary microglia stained with the activation marker CD45 show an increase in CD45-immunoreactive microglia in lenti-GFP infected cells treated with TNF but not in lenti-DN-TNF infected cells treated with TNF. Scale bar = 50 μm. (C) Quantification of TNF-induced microglia activation in lenti-DN-TNF versus lenti-GFP or mock-transduced 3xTgAD primary microglia cultures. Total microglia (all $CD45_{low+high}$ positive cells) and activated microglia ($CD45_{high}$ cells with nuclear enrichment of CD45) were counted. Values shown are percent activated microglia ($CD45_{high}/CD45_{low+high}$) × 100 ± S.E.M., * denotes significantly different from mock-infected/vehicle-treated at $p < 0.05$ by one-way ANOVA followed by Tukey's post-hoc test.

were performed to deliver the lentivirus bilaterally and maximize virus spread. Lentivirus-based DN-TNF (or GFP) expression was allowed to proceed for 6 weeks prior to the start of the chronic systemic inflammatory stimulus, which consisted of intraperitoneal injections of 7.5×10^5 E.U./kg of LPS twice a week for another 6 weeks, an experimental paradigm previously reported to hasten the appearance of AD-like pathology in 3xTgAD mice (Kitazawa et al., 2005) (Fig. 4A). The efficiency of lentiviral transduction of cells in the brains of mice injected with lenti-DN-TNF ICV was assessed by immunohistochemical analysis with an anti-GFP antibody to detect expression from the lentiviral vector. GFP-immunoreactivity was readily and specifically detected in the brain parenchyma of mice injected with lenti-DN-TNF, confirming that transduced brain cells were indeed expressing the proteins encoded by the lentivirus (Fig. 4B). In support of our hypothesis that TNF is a key mediator of the enhanced amyloid-associated pathology induced by chronic systemic inflammation, the brains of mice injected with lenti-DN-TNF displayed a drastic reduction in intraneuronal APP-derived 6E10-immunoreactive species in parietal cortex (Fig. 5A, black brackets), in the CA1 region of the hippocampus (Fig. 5A, white brackets), in amygdala (Fig. 5B) and in entorhinal and temporal cortex (not shown) compared to mice injected with the control lenti-GFP. We performed unbiased stereology to estimate the number of 6E10-immunoreactive cells in the hippocampus, cortex and amygdala using the optical fractionator method, and found that lenti-DN-TNF-transduced brains displayed a significant (~60%) reduction in accumulation of intraneuronal APP-derived 6E10-immunoreactive protein compared to lenti-GFP transduced brains ($p<0.05$ by one-tailed Student's *t*-test) (Fig. 5C). Therefore, we concluded that *in vivo* inhibition of TNF signaling via infusion of XENP345 or transduction with lenti-DN-TNF results in significant attenuation of 6E10-immunoreactive protein.

Given that immunoreactivity for 6E10 can represent APP, C-terminal APP fragments, and/or Aβ peptides, we performed brightfield immunohistology to investigate if the intraneuronal APP-derived 6E10-immunoreactive species in brains of young adult 3xTgAD mice exposed to chronic systemic inflammation was composed of mainly Aβ peptides. We stained intervening brain sections with Aβ40- and Aβ42-specific antibodies from two independent sources to compare the staining patterns with that of the 6E10. Brightfield immunohistological analysis of hippocampal brain regions with Aβ40 and Aβ42 antibodies revealed no detectable immunoreactivity in neuronal populations which were clearly positive for 6E10 in young-adult 3xTgAD mice that received chronic systemic LPS injections and either saline infusion via osmotic pump in the hippocampus CA1 region (Supplementary Fig. S3A) or lenti-GFP (Supplementary Fig. S3B) as negative controls for XENP345 and lenti-DNTNF, respectively. As a positive control for the Aβ40 and Aβ42 antibodies, hippocampal brain regions from an untreated APPswe/PS1Δ9 transgenic mouse were analyzed in the same way and found to display identical staining patterns for 6E10, Aβ40 and Aβ42 in and around amyloid plaque deposits (Supplementary Fig. S3C). We considered that our inability to detect Aβ40 and Aβ42 peptides using brightfield immunohistology could be due to the reduced sensitivity of the technique. To test this possibility, we performed double immunofluorescence labeling of hippocampal sections with the 6E10 antibody (red) and a C-terminal-specific APP antibody (green) to generate confocal images and construct Z-stack series in order to determine the relative abundance of Aβ peptides (6E10 signal minus the C-terminal-specific signal subtracted) versus β-CTF, α-CTF, and APP in our 3xTgAD mice (see Materials and methods). The levels of APP/β-CTF species (regions positive for both 6E10 and C-terminal immunoreactivity, yellow overlay signal) were detectably higher than those of Aβ (shown as Aβ subtracted signal) in young adult 3xTgAD mice transduced with lenti-DN-TNF and exposed to chronic systemic inflammation (Fig. 6A). Consistent with previous observations that chronic systemic LPS did not significantly increase Aβ levels measured by ELISA (Kitazawa et al., 2005), this confocal subtraction analysis indicated that chronic exposure to systemic LPS did not significantly increase the levels of Aβ peptides and inhibition of TNF signaling with the DN-TNF inhibitor XENP345 (Fig. 6B, $p=0.34$ by Kruskal–Wallis analysis) or with lenti-DN-TNF (Fig. 6C, $p=0.15$ by Kruskal–Wallis analysis) had no effect on their levels either. To confirm these observations biochemically, we performed quantitative high-sensitivity ELISAs for soluble and insoluble Aβ40 and 42 in lysates of microdissected cortices and hippocampi from 3xTgAD mice injected with lenti-DN-TNF (or lenti-GFP) and exposed to chronic systemic inflammation. In agreement

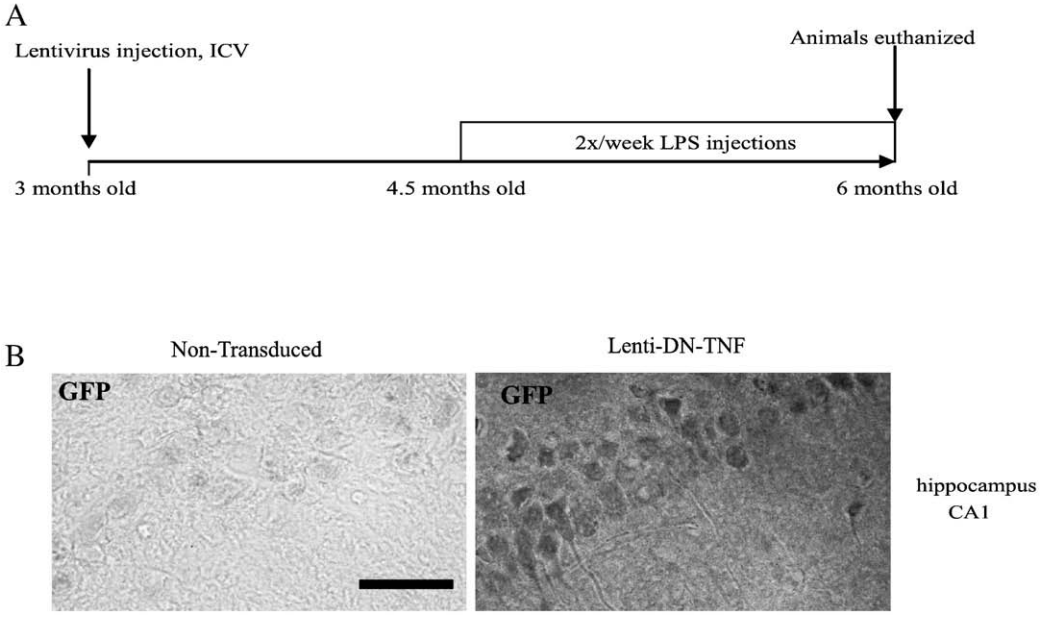

Fig. 4. ICV administration of Lenti-DN-TNF results in detectable *in vivo* expression in 3xTgAD mice. (A) Schematic of experimental design: 3 month-old 3xTgAD mice received an ICV injection of lenti-DN-TNF or lenti-GFP. At 4.5 months old, mice received a bi-weekly regimen of intraperitoneal (i.p.) LPS (7.5×10^5 E.U./kg) injections for 6 weeks. Tissue was harvested at the time mice were 6 months old. (B) Immunohistological analysis of anti-GFP immunoreactivity in the hippocampus of lenti-DN-TNF-IRES-GFP transduced mouse brain, but not in non-transduced mouse brains, confirms expression of the lentiviral-encoded genes. Scale bar = 100 μm.

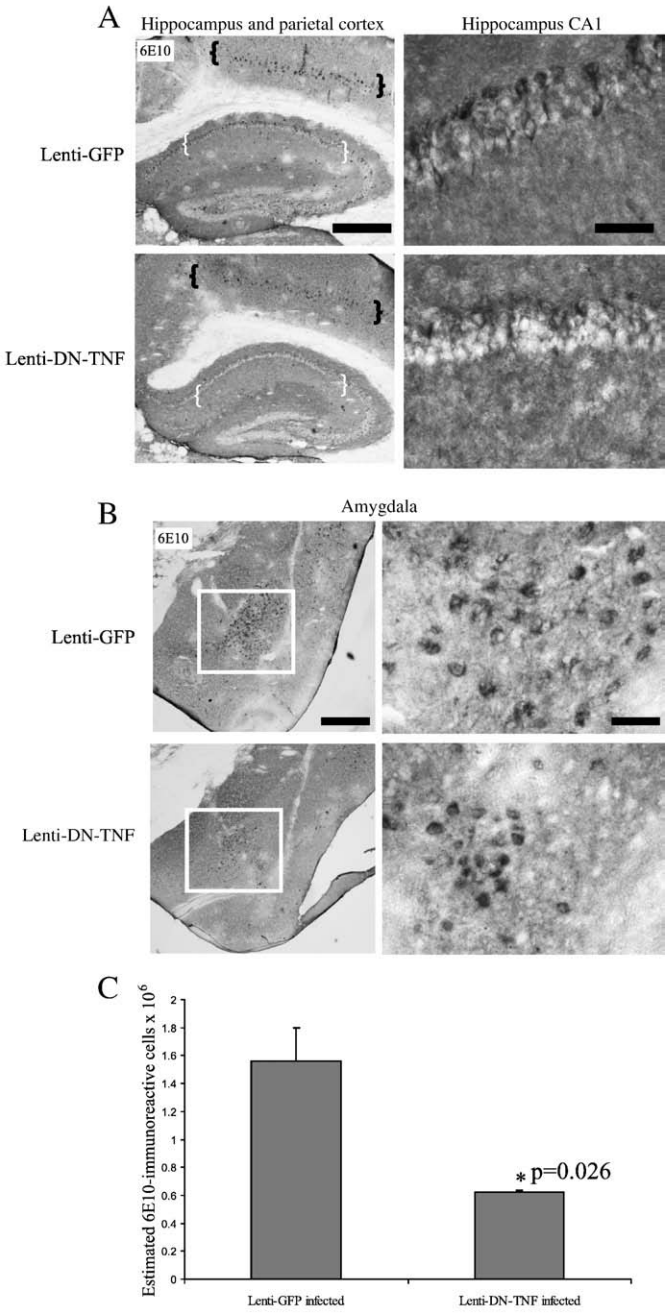

Fig. 5. ICV administration of lenti-DN-TNF attenuates accumulation of intraneuronal 6E10-immunoreactive protein(s) in 3xTgAD mice. (A) Brains of 3xTgAD mice that received lenti-GFP and chronic LPS exposure display accumulation of intraneuronal 6E10-immunoreactive amyloid-associated protein(s) in layer V of parietal cortex (enclosed by black curly brackets) and in the hippocampus, CA1 region (enclosed by white curly brackets) shown on the left at 4× magnification, scale bar = 500 μm; and on the right at 40× magnification, scale bar = 50 μm. Brains of 3xTgAD mice that received lenti-DN-TNF and chronic LPS exposure display reduced accumulation of intraneuronal 6E10-immunoreactive amyloid-associated protein(s) in both parietal cortex and hippocampus. (B) Brains of 3xTgAD mice that received lenti-DN-TNF and chronic LPS exposure display marked reduction of intraneuronal 6E10-immunoreactive protein(s) in the amygdala compared to animals that received lenti-GFP ICV and chronic LPS i.p. injections. On the left 4× magnification, medial amygdala enclosed in a white rectangle, scale bar = 500 μm; on the right 40× magnification, scale bar = 50 μm. (C) Stereological analysis of the number of 6E10-immunoreactive neurons in hippocampus and cortex of 3xTgAD mice that received lenti-GFP/LPS or lenti-DN-TNF/LPS. Values shown are group means ± SEM. for $n = 3$ animals, * denotes $p = 0.026$ by one-tailed t-test.

with our confocal analyses of hippocampal brain sections, we found that levels of Aβ40 and Aβ42 were low and not significantly changed by TNF signaling inhibition (Fig. 6D, one-way ANOVA, $n = 4$ for lenti-DN-TNF, $n = 3$ for lenti-GFP, Aβ40 $p = 0.12$; Aβ42 $p = 0.10$). Taken together, results from these multiple independent approaches led us to conclude that the bulk of the 6E10-IR species that accumulated intraneuronally as a result of the chronic systemic inflammatory stimulus and was significantly attenuated when solTNF signaling was inhibited was likely to be APP or β-CTF.

Inhibition of TNF signaling prevents accumulation of intraneuronal C9-immunoreactive protein elicited by chronic exposure to systemic inflammation

To confirm that the major fraction of 6E10-IR protein was APP or β-CTF, we used the C-terminal APP antibody C9 (Kimberly et al., 2005) to stain brain sections of treated 3xTgAD mice. We compared brain sections stained with C9 from animals fitted with osmotic pumps delivering DN-TNF and treated with LPS to those from animals fitted with osmotic pumps delivering saline and treated with LPS. We also compared hippocampal CA1 brain sections stained with C9 from 3xTgAD mice that received lenti-GFP injections followed by systemic LPS with those of mice that received lenti-DN-TNF followed by systemic LPS. In agreement with 6E10-IR results, accumulation of intraneuronal APP C9-immunoreactive material in the hippocampus CA1 region was evident in 3xTgAD mice that were fitted with a saline pump in the CA1 and injected with low-dose LPS (i.p.) and this increase was inhibited by infusion of XENP345 (Fig. 7A). Similarly, lenti-DN-TNF/LPS-treated mice displayed reduced C9-immunoreactivity in the parietal cortex and hippocampus CA1 region compared to lenti-GFP/LPS-treated mice (Fig. 7B), suggesting that TNF signaling is a critical step in this process. Given the overlapping immunohistological pattern between 6E10 and C9 and the position of the epitopes for 6E10 and C9 on the APP protein, our data suggests that the bulk of the accumulated 6E10-immunoreactive protein species is likely to be composed of full-length APP and/or β-CTF and a small amount of Aβ peptides. To directly investigate whether full length was one of the 6E10-immunoreactive species accumulating intraneuronally in LPS-treated mice, we stained brain sections from our experimental animals as well as some APP_{swe}/PS1Δ9 mice using two separate antibodies against the N-terminus of APP. An antibody obtained from Sigma (cat. #A8967) failed to stain N-terminal APP in either 3xTgAD or APP_{swe}/PS1Δ9 brain sections. However, immunohistological analysis with 22C11 anti-N-terminal APP antibody yielded a punctate pattern in neurons in brain sections from APP_{swe}/PS1Δ9 mice (positive control) but failed to detect robust intraneuronal staining in the brains of 3xTgAD mice treated with LPS systemically (data not shown). Taken together with results from confocal analyses these data led us to conclude that the 6E10-immunoreactive species is not full-length APP but rather mostly β-CTF, (recognized by 6E10 and C9) and some α-CTF (recognized only by C9). Next, we aimed to extend and confirm these findings using a biochemical approach. Densitometric analyses of immunoblots of whole-hippocampus and cortex detergent lysates from lenti-GFP and lenti-DN-TNF-injected animals revealed no significant differences in protein levels of full-length APP, the various APP-derived species, BACE1, or presenilin-1 (PS1), the catalytic subunit of γ-secretase between the mice exposed to chronic systemic LPS and injected with lenti-GFP versus lenti-DN-TNF (Supplementary Fig. S4). However, given that immunohistological analyses 6E10 and C9 indicate that only a subpopulation of cells displays robust accumulation of the APP-derived species, it is not surprising that the effects of TNF signaling inhibition on this sub-population cannot be appreciated in the background of many other cells which are not affected. On the basis of these results, we concluded that inhibition of TNF signaling by gene transfer of DN-TNF via lentivirus prevents LPS-induced intraneuronal accumulation of β-CTF to the same extent as that achieved with chronic delivery of the DN-TNF biologic XENP345. Taken together, these findings suggest that persistent inactivation of TNF signaling during the early stages of AD-like amyloid

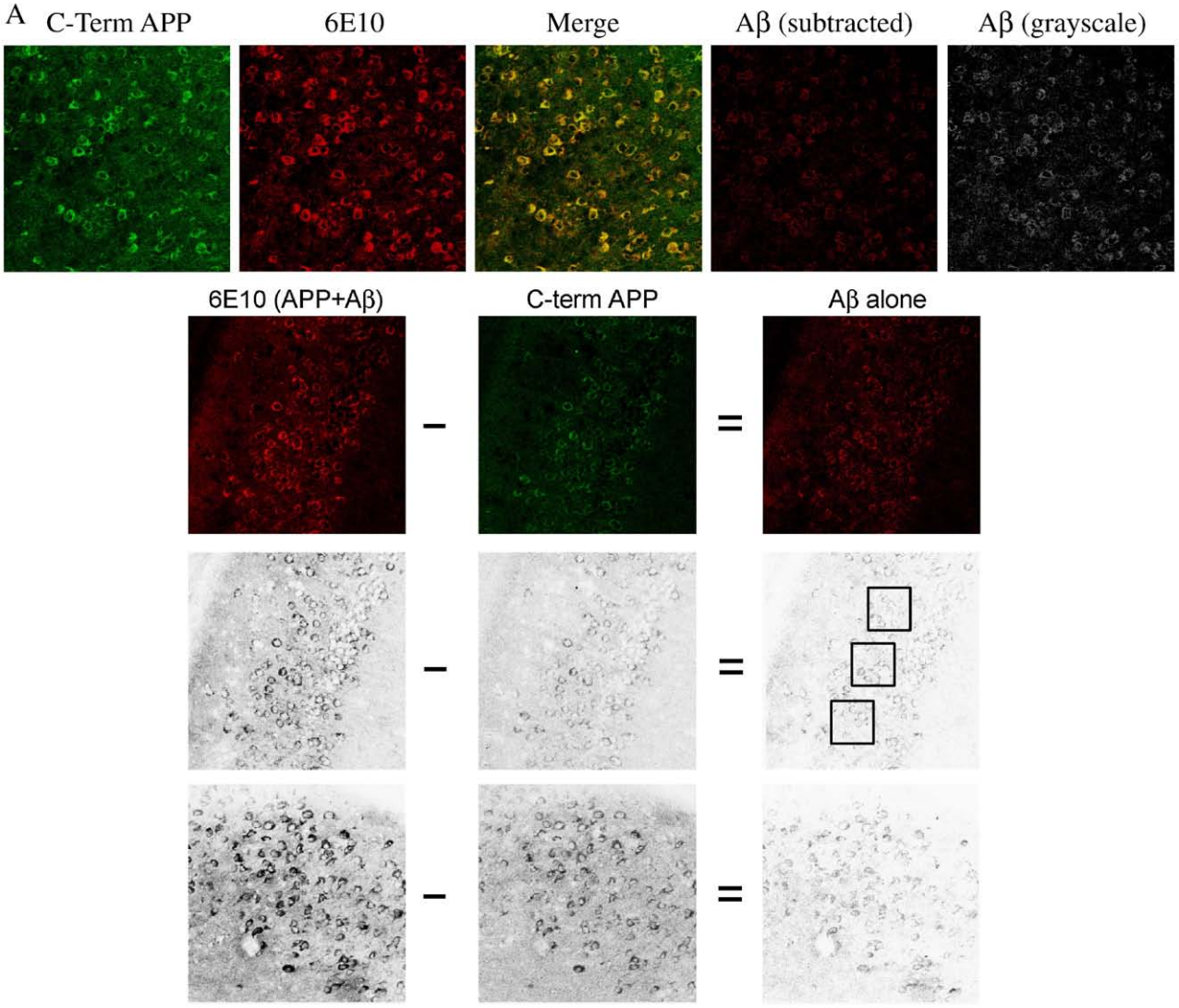
A
C-Term APP
6E10
Merge
Aβ (subtracted)
Aβ (grayscale)
6E10 (APP+Aβ)
C-term APP
Aβ alone

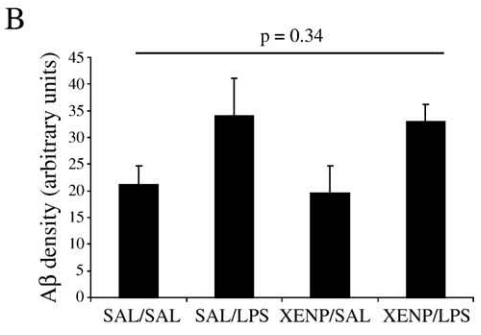
B
p = 0.34
Aβ density (arbitrary units)
SAL/SAL
SAL/LPS
XENP/SAL
XENP/LPS

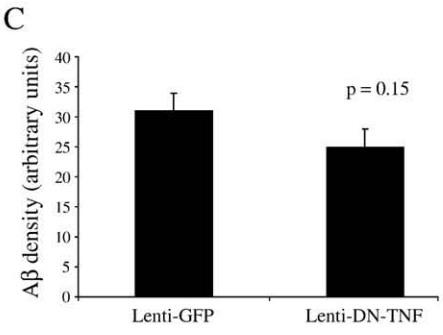
C
p = 0.15
Aβ density (arbitrary units)
Lenti-GFP
Lenti-DN-TNF

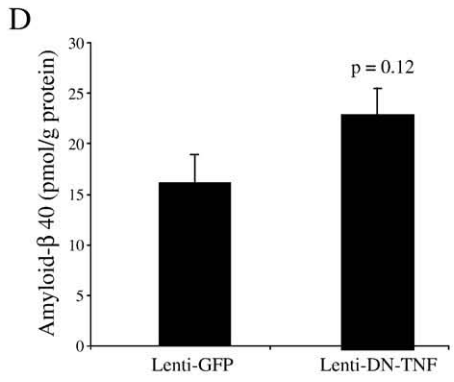
D
p = 0.12
Amyloid-β 40 (pmol/g protein)
Lenti-GFP
Lenti-DN-TNF

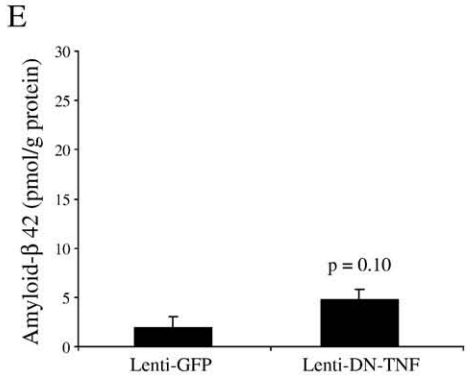
E
p = 0.10
Amyloid-β 42 (pmol/g protein)
Lenti-GFP
Lenti-DN-TNF

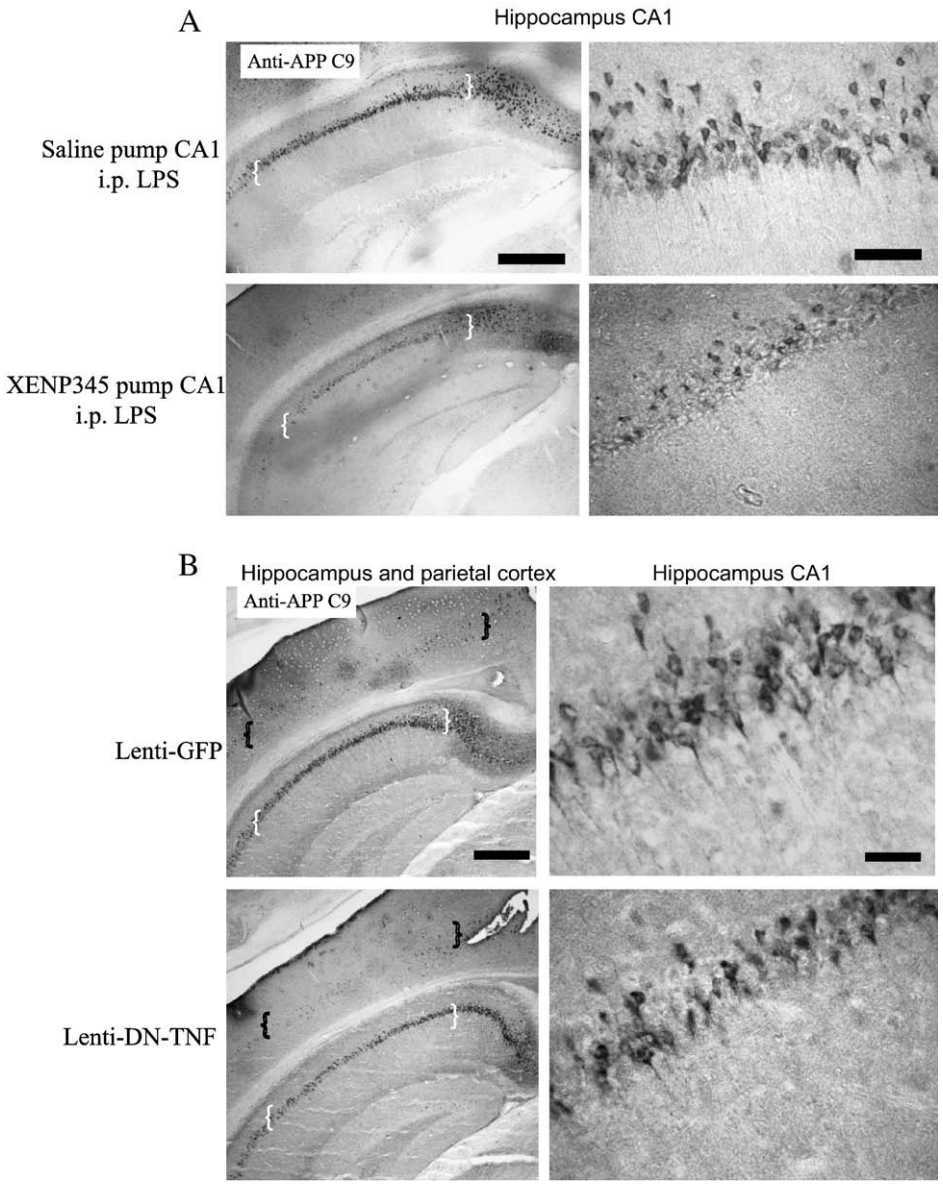

Fig. 7. SolTNF inhibition reduces accumulation of β-CTF and/or APP. (A) Brains of 3xTgAD mice that received lenti-GFP and chronic systemic LPS injections display accumulation of intraneuronal anti-APP C9-immunoreactive material in layer V of parietal cortex (surrounded by black curly brackets) and in the CA1 region of the hippocampus (surrounded by white curly brackets); C9 immunoreactivity is attenuated by lenti-DN-TNF ICV transduction. On the left, 4× magnification: scale bar = 500 μm; On the right, 40× magnification: scale bar = 50 μm. (B) 3xTgAD mice that were injected with low-dose LPS i.p. show increased 6E10-immunoreactive protein in the CA1 region of the hippocampus surrounded by curly brackets; this increase is inhibited by chronic infusion of the solTNF-selective inhibitor XENP345. On the left, 4× magnification, scale bar = 500 μm; on the right, 40× magnification, scale bar = 50 μm.

neuropathology may be an effective way to block the cascade of downstream events (such as accumulation of toxic APP-derived fragments and/or overproduction of Aβ oligomers) that contribute to cognitive decline.

As expected, microglial activation (measured by CD45 and CD68 immunohistology) induced by chronic systemic LPS was not completely inhibited by *in vivo* infusion of XENP345 or lenti-DN-TNF transduction (Supplementary Fig. S5). This result is not surprising given that LPS elicits production of many other inflammatory factors that can also activate microglia *in vivo*. In addition, these findings are consistent with our previously published work in a rat model of Parkinson's disease (McCoy et al., 2006) in which XENP345 neutralized solTNF produced in response to LPS and rescued dopaminergic neurons despite persistent microglia activation.

Fig. 6. Relative abundance of APP, C-terminal APP fragments (β-CTF and α-CTF), and Aβ peptides and quantification of Aβ40 and Aβ42 by densitometry and ELISA in LPS-treated 3xTgAD mice transduced with lenti-GFP or lenti-DN-TNF. (A) Immunofluorescent confocal Z-slice images of hippocampal sections double-labeled with 6E10 (red) and a C-terminal fragment (CTF) specific APP antibody (green) were taken to construct a Z-stack to establish the relative abundance of Aβ (6E10+/CTF−, red only), APP/β-CTF (6E10+/CTF+, yellow) and α-CTF (6E10−/CTF+, green only) in 3 equal size square fields per animal which were averaged and compared by *t*-test in 3xTgAD mice from various treatment groups. Results indicate lower abundance of Aβ and higher abundance of APP/β-CTF species (6E10+/CTF+, yellow). Densitometric analysis of Aβ only signal in brain sections of (B) animals infused with XENP345 (or saline as negative control) or (C) injected with lenti-DN-TNF (or lenti-GFP as negative control) and subjected to chronic systemic inflammation indicate TNF signaling inhibition has minimal effect on Aβ levels in (B) mice fitted with osmotic pumps ($p = 0.34$, Kruskal–Wallis) or (C) in lenti-injected mice ($p = 0.15$, Kruskal–Wallis). Quantitative ELISAs for (D) Aβ40 and (E) Aβ42 revealed low but detectable levels of both peptides and no significant difference between lenti-DN-TNF and lenti-GFP-treated 3xTgAD mice. One-way ANOVA, $n = 4$ for lenti-DN, $n = 3$ for lenti-GFP, Aβ40 $p = 0.12$; Aβ42 $p = 0.10$.

Genetic inactivation of TNF signaling in 3xTgAD mice prevents accumulation of intraneuronal 6E10 and C9-immunoreactivity induced by chronic systemic inflammation

Genetic deletion of the TNF receptor gene *Tnfrsf1a* in APP 23 transgenic mice was recently shown to result in reduction of both the number of amyloid plaques and the cognitive deficits in these mice (He et al., 2007). Therefore, we took the same genetic approach in the 3xTgAD mice and inactivated solTNF signaling by crossing these mice to TNFR1-deficient mice or to WT mice of the same genetic background (C57/B6) and bred the compound transgenics to homozygosity. We then examined intraneuronal APP-derived amyloid burden in the brains of TNFR1-deficient 3xTgAD mice and 3xTgAD; WT B6 mice exposed to chronic systemic inflammation (or given saline i.p. injections) for 6 wks. Consistent with results obtained after chronic inhibition of solTNF signaling with XENP345 or lenti-DN-TNF, 3xTgAD;WT B6 mice given i.p. LPS injections displayed increased intraneuronal 6E10 and C9-immunoreactivity whereas inactivation of TNFR1 in 3xTgAD mice prevented this intraneuronal accumulation. Interestingly, 6E10 immunoreactivity was not absent from the sections; instead, it was detectable in cellular processes characteristic of microglia and may represent engulfed Aβ (Fig. 8).

Discussion

The accumulation of intraneuronal APP/Aβ reported in brains of AD patients and several transgenic mouse models with AD-like pathology may be early events that promote neuronal dysfunction and death (Chin et al., 2007; Gouras et al., 2000; LaFerla et al., 1997). By blocking TNF signaling transiently (4 weeks) with solTNF-selective dominant negative TNF (DN-TNF) inhibitor XENP345 or persistently with a lentivirus encoding DN-TNF, we reduced the accumulation of intraneuronal APP β-CTF in the AD-affected brain regions of LPS-treated 3xTgAD mice. Previous studies in the 3xTgAD model reported that TNF mRNA is increased in entorhinal cortex at 3 months (Janelsins et al., 2005) prior to the onset of the cognitive deficits that

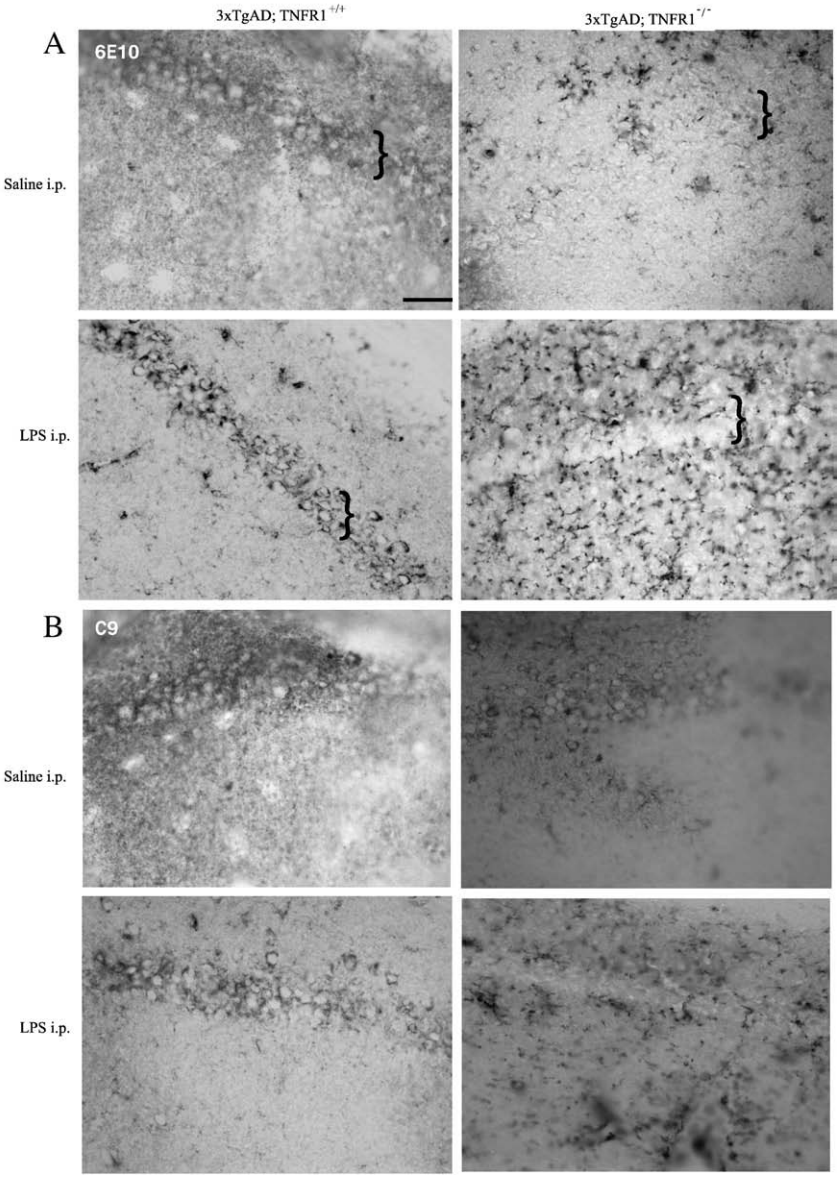

Fig. 8. Genetic deletion of TNFR1 in 3xTgAD transgenic mice prevents accumulation of intraneuronal 6E10 immunoreactivity in response to chronic systemic inflammation. Compound transgenic mice were generated by crossing 3xTgAD mice with TNFR1-deficient (TNFR1−/−) mice or with WT mice of the same genetic background (C57B6/J, TNFR1+/+). Immunohistological analysis revealed intraneuronal accumulation of (A) 6E10 and (B) C9-immunoreactive amyloid-associated proteins in 3xTgAD;TNFR1+/+ mice that received chronic systemic LPS injections but not in 3xTgAD;TNFR1−/− mice which lack functional solTNF signaling. 40× magnification, scale bar=50 μm.

correlate with the appearance of intraneuronal APP-derived 6E10-IR protein species. Therefore, we hypothesized that TNF upregulation and the appearance of that intraneuronal amyloid-associated species were causally linked. We further reasoned that targeted inhibition of TNF signaling in AD-relevant brain regions may be an effective basis to halt or attenuate progression of amyloid-associated neuropathology prior to the appearance of extracellular plaques. Our results demonstrate that both chronic infusion into the hippocampal region of 3xTgAD mice of a novel dominant negative biologic selective for soluble TNF (Zalevsky et al., 2007) and persistent inactivation of TNF signaling with a lentiviral-encoded DN-TNF drastically reduced accumulation of intraneuronal β-CTF in the brains of 3xTgAD mice exposed to chronic systemic inflammation as measured by 6E10 and C9 immunohistochemistry. Lastly, genetic deletion of TNFR1 in 3xTgAD mice prevented the LPS-induced accumulation of β-CTF. β-CTF alters ionic homeostasis (Fraser et al., 1997) and is neurotoxic in differentiated PC12 cells (Yankner et al., 1989) and in transgenic mice expressing the C-terminus of APP (Oster-Granite et al., 1996). Neuronal cells bearing familial AD (FAD) mutations accumulate β-CTF intracellularly (McPhie et al., 1997), implicating its involvement in AD pathogenesis.

Previous studies measuring reduced amyloid burden after genetic ablation of TNFR1 in APP23 transgenic mice have implicated TNF or one of its downstream targets in modulation of amyloid-associated neuropathology (Ohno et al., 2007); but this is the first study that selectively inhibits soluble TNF signaling in an acute manner in adult animals with a resulting effect on intraneuronal β-CTF. By using both a selective anti-TNF biologic and a gene transfer approach, we were able to time the inhibition of TNF to a relevant and precise interval in the progressive AD-like pathology in 3xTgAD mice; i.e., when TNF is upregulated and intraneuronal 6E10-IR protein first appears (Billings et al., 2005; Janelsins et al., 2005). As such, our findings provide strong rationale to further explore practical ways to deliver highly selective soluble TNF inhibitors such as DN-TNF biologics to the CNS for potential use in neurodegenerative diseases associated with chronic neuroinflammation. We have previously investigated the efficacy of XENP345 in other models of neurodegeneration and demonstrated that inhibition of solTNF signaling rescued approximately 50% of the rat dopaminergic neurons that would otherwise die as a result of 6-hydroxydopamine- or LPS-induced death in models of Parkinson's disease (McCoy et al., 2006).

The DN-TNF variant we used, XENP345, is a mutant form of human solTNF with disrupted receptor-ligand interfaces (Steed et al., 2003; Zalevsky et al., 2007). It has been shown specifically to neutralize solTNF signaling by forming dominant negative heterotrimers that have significantly attenuated binding affinity for TNF receptors (Steed et al., 2003; Zalevsky et al., 2007) thereby lowering the effective concentration of solTNF without affecting overall production levels of TNF or the biological activity of transmembrane TNF (tmTNF), including its role in maintaining innate immunity (Zalevsky et al., 2007). SolTNF signals primarily through TNFR1 (Grell et al., 1998) and tmTNF signals primarily through TNFR2 (Grell et al., 1995). Therefore, selectivity of DN-TNF for solTNF may be highly relevant in the context of the brain and specifically the hippocampus, considering that TNF signaling through TNFR2 is protective against glutamate excitotoxicity (Marchetti et al., 2004), reduces seizures in response to kainic acid (Balosso et al., 2005), and most likely promotes the survival of hippocampal neuroblasts after ischemic injury (Heldmann et al., 2005). Systemic administration of drugs that inhibit both tmTNF and solTNF, such as etanercept or infliximab, have been associated with serious side effects including an increased susceptibility to infection and demyelinating disease (Scheinfeld, 2004). These effects may be related to the ability of these biologics to inhibit tmTNF signaling, which plays an important role in resolving inflammation and maintaining immunity to certain pathogens (Alexopoulou et al., 2006). Alternatively, introduction of the DN-TNF sequence into a lentiviral vector may provide several advantages over chronic infusion of DN-TNF biologics. Lentiviruses allow for long-term expression of encoded proteins (Blomer et al., 1997; Jakobsson and Lundberg, 2006), and a targeted lentiviral injection will afford long-term inhibition of TNF signaling in a specific brain region without the invasiveness of a chronic infusion pump. In the future, inducible viral vectors may permit precisely timed delivery of the drug (Blesch et al., 2005) while circumventing the inherent limitations of using a chronic infusion device.

The association between neuroinflammation and neurodegenerative diseases, including AD, has been investigated extensively (Eikelenboom et al., 2006; Griffin, 2006; Hoozemans et al., 2006; McGeer and McGeer, 2003; Mrak and Griffin, 2005; Wyss-Coray and Mucke, 2002). Epidemiological studies suggest a link between chronic use of non-steroidal anti-inflammatory drugs (NSAIDs) and reduced risk for AD, but thus far clinical trials using systemic administration have yielded mixed or inconclusive results (Launer, 2003; McGeer and McGeer, 2007; van Gool et al., 2003), reflecting the need to identify and target the key inflammatory mediators that promote amyloid-associated neuropathology. Our *in vivo* findings provide strong support for TNF as a critical inflammatory modulator of APP turnover and/or modulation of early amyloid-associated pathology in hippocampal and cortical neurons. Interestingly, neuronal expression of hAPP/Aβ in the J20 transgenic model of AD has been shown to be sufficient to reduce Reelin expression in a specific population of entorhinal cortical pyramidal neurons *in vivo* and qualitatively similar reductions of Reelin-expressing pyramidal neurons have been reported in the entorhinal cortex of AD brains (Chin et al., 2007). Therefore, one speculative possibility raised by our findings that will need to be addressed in future studies is that neuroinflammatory processes may contribute to accelerated cognitive decline in AD by driving TNF-dependent intraneuronal accumulation of APP β-CTF in Reelin-positive interneurons and promoting abnormal Reelin processing.

Activated microglia cluster around amyloid plaques (McGeer et al., 1987), and β-secretase (BACE1) has been shown to be upregulated in neuronal populations that are in close proximity to amyloid plaques (Zhao et al., 2007). Physiologically, one of the main effector pathways downstream of TNF (Hohmann et al., 1990), the NFκB pathway, can regulate BACE1 expression after exposure to Aβ (Bourne et al., 2007). Mechanistically, genetic ablation of BACE1 in the 5xFAD APP/PS1 transgenic mouse a model of AD resulted in marked reduction of amyloid burden, neuron loss and cognitive deficits (Ohno et al., 2007). Given that TNF can affect Aβ production (Blasko et al., 1999, 2000) through upregulation of BACE1 expression (Yamamoto et al., 2007) and γ-secretase activity (Liao et al., 2004) as well as expression of APP itself (Lahiri et al., 2003), our findings support an important role for TNF-dependent regulation of APP processing *in vivo* and underscore the importance of targeting molecular mediators that promote BACE1 activity to pathophysiological levels. In support of this idea, genetic deletion of the TNF receptor gene *Tnfrsf1a* in APP 23 transgenic mice resulted in reduced amyloid plaque number and cognitive deficits in these mice (He et al., 2007).

Although our biochemical and immunohistological analyses did not reveal robust accumulation of Aβ peptides in 3xTgAD mice under basal conditions or in response to chronic systemic inflammation, our studies strongly suggest that it may be feasible to selectively target solTNF therapeutically to prevent dysregulated APP turnover and/or transport induced by chronic neuroinflammation, thereby halting or attenuating disease progression and cognitive impairment. It has been proposed that in advanced stages of AD once extensive amyloid plaques have formed, elevated levels of pro-inflammatory cytokines, including TNF, may inhibit phagocytosis of toxic Aβ species and/or hinder efficient plaque removal by brain resident microglia (Koenigsknecht-Talboo and Landreth, 2005). If abnormal APP turnover/processing and/or intraneuronal accumulation of APP,

APP C-terminal fragments, or Aβ can be blocked in the earliest stages of AD with solTNF-selective inhibitors, we speculate that it may also be possible to prevent or significantly delay appearance of extracellular plaques and tau pathology given that Aβ pathology has been shown to influence the progression of tau pathology (Gotz et al., 2001; Lewis et al., 2001). In support of this idea, chronic elevation of TNF signaling in the hippocampus of 3xTgAD mice achieved via adeno-associated virus enhanced the appearance of intraneuronal amyloid and hyperphosphorylated tau ultimately leading to neuronal death (Janelsins et al., 2008). In conclusion, our findings offer support for two novel and specific approaches to inhibit the accumulation of intraneuronal amyloid-associated proteins triggered by chronic systemic inflammation, and provide further proof-of-concept that solTNF is a valid therapeutic target to modify disease progression during the early stages of AD.

Acknowledgments

The authors would like to thank D. E. Szymkowski of Xencor, Inc. for providing us with the DN-TNF biologic XENP345 and J. Zalevsky of Xencor, Inc. for the plasmids containing the DN-TNF sequence. We thank M. Lavoie and D. Selkoe of Harvard Medical School and Brigham and Women's Hospital for the anti-APP C9 antibody; R. Vassar of the Northwestern Feinberg School of Medicine for the anti-BACE1 antibody; R. Bachoo and L. Loomis for their gift of the SS01 murine astrocyte cell line; B. R. Botterman, K.E. Tansey, and C. Wang for assistance with stereotaxic surgeries; B. Pearson, Isaac Treviño, and T.C. Frank-Cannon for assistance with immunohistochemical techniques and statistical analyses, M.K. McCoy for assistance with TNF ELISAs, and members of the Tansey lab for insightful discussions. This work was supported by an Alzheimer's disease research grant from the American Health Assistance Foundation (MGT), the Alzheimer's Disease Center at UT Southwestern (NIA, NIH P30AG12300), and NIH pre-doctoral training grant T32 GM 008203 (FEM).

Appendix A. Supplementary data

Supplementary data associated with this article can be found, in the online version, at doi:10.1016/j.nbd.2009.01.006.

References

Aggarwal, B.B., Samanta, A., Feldmann, M., 2000. TNFa. In: Oppenheim, M.L.J.J. a. F. (Ed.), Cytokine Reference. Academic Press, pp. 414–434.
Akiyama, H., et al., 2000. Inflammation and Alzheimer's disease. Neurobiol. Aging 21, 383–421.
Alexopoulou, L., et al., 2006. Transmembrane TNF protects mutant mice against intracellular bacterial infections, chronic inflammation and autoimmunity. Eur. J. Immunol. 36, 2768–2780.
Alvarez, A., et al., 2007. Serum TNF-alpha levels are increased and correlate negatively with free IGF-I in Alzheimer disease. Neurobiol. Aging 28, 533–536.
Balosso, S., et al., 2005. Tumor necrosis factor-alpha inhibits seizures in mice via p75 receptors. Ann. Neurol. 57, 804–812.
Billings, L.M., et al., 2005. Intraneuronal Abeta causes the onset of early Alzheimer's disease-related cognitive deficits in transgenic mice. Neuron 45, 675–688.
Blasko, I., et al., 1999. TNFalpha plus IFNgamma induce the production of Alzheimer beta-amyloid peptides and decrease the secretion of APPs. FASEB J. 13, 63–68.
Blasko, I., et al., 2000. Costimulatory effects of interferon-gamma and interleukin-1beta or tumor necrosis factor alpha on the synthesis of Abeta1–40 and Abeta1–42 by human astrocytes. Neurobiol. Dis. 7, 682–689.
Blesch, A., et al., 2005. Regulated lentiviral NGF gene transfer controls rescue of medial septal cholinergic neurons. Molec. Ther. 11, 916–925.
Blomer, U., et al., 1997. Highly efficient and sustained gene transfer in adult neurons with a lentivirus vector. J. Virol. 71, 6641–6649.
Bourne, K.Z., et al., 2007. Differential regulation of BACE1 promoter activity by nuclear factor-kappaB in neurons and glia upon exposure to beta-amyloid peptides. J. Neurosci. Res. 85, 1194–1204.
Cai, X.D., et al., 1993. Release of excess amyloid beta protein from a mutant amyloid beta protein precursor. Science 259, 514–516.
Chin, J., et al., 2007. Reelin depletion in the entorhinal cortex of human amyloid precursor protein transgenic mice and humans with Alzheimer's disease. J. Neurosci. 27, 2727–2733.
Citron, M., et al., 1992. Mutation of the beta-amyloid precursor protein in familial Alzheimer's disease increases beta-protein production. Nature 360, 672–674.
Collins, J.S., et al., 2000. Association of a haplotype for tumor necrosis factor in siblings with late-onset Alzheimer disease: the NIMH Alzheimer Disease Genetics Initiative. Am. J. Med. Genet. 96, 823–830.
Das, P., et al., 2003. Amyloid-beta immunization effectively reduces amyloid deposition in FcRgamma−/− knock-out mice. J. Neurosci. 23, 8532–8538.
Eikelenboom, P., et al., 2006. The significance of neuroinflammation in understanding Alzheimer's disease. J. Neural Transm. 113, 1685–1695.
Estus, S., et al., 1992. Potentially amyloidogenic, carboxyl-terminal derivatives of the amyloid protein precursor. Science 255, 726–728.
Fillit, H., et al., 1991. Elevated circulating tumor necrosis factor levels in Alzheimer's disease. Neurosci. Lett. 129, 318–320.
Flick, D.A., Gifford, G.E., 1986. Production of tumor necrosis factor in unprimed mice: mechanism of endotoxin-mediated tumor necrosis. Immunobiology 171, 320–328.
Frank, T.C., et al., 2003. Fluoro-jade identification of cerebellar granule cell and Purkinje cell death in the alpha1A calcium ion channel mutant mouse, leaner. Neuroscience 118, 667–680.
Fraser, S.P., et al., 1997. Ionic effects of the Alzheimer's disease beta-amyloid precursor protein and its metabolic fragments. Trends Neurosci. 20, 67–72.
Goate, A., et al., 1991. Segregation of a missense mutation in the amyloid precursor protein gene with familial Alzheimer's disease. Nature 349, 704–706.
Gotz, J., et al., 2001. Formation of neurofibrillary tangles in P301l tau transgenic mice induced by Abeta 42 fibrils. Science 293, 1491–1495.
Gouras, G.K., et al., 2000. Intraneuronal Abeta42 accumulation in human brain. Am. J. Pathol. 156, 15–20.
Grell, M., et al., 1995. The transmembrane form of tumor necrosis factor is the prime activating ligand of the 80 kDa tumor necrosis factor receptor. Cell 83, 793–802.
Grell, M., et al., 1998. The type 1 receptor (CD120a) is the high-affinity receptor for soluble tumor necrosis factor. Proc. Natl. Acad. Sci. U. S. A. 95, 570–575.
Griffin, W.S., 2006. Inflammation and neurodegenerative diseases. Am. J. Clin. Nutr. 83, 470S–474S.
Haass, C., et al., 1993. beta-Amyloid peptide and a 3-kDa fragment are derived by distinct cellular mechanisms. J. Biol. Chem. 268, 3021–3024.
He, P., et al., 2007. Deletion of tumor necrosis factor death receptor inhibits amyloid {beta} generation and prevents learning and memory deficits in Alzheimer's mice. J. Cell Biol. 178, 829–841.
Heldmann, U., et al., 2005. TNF-alpha antibody infusion impairs survival of stroke-generated neuroblasts in adult rat brain. Exp. Neurol. 196, 204–208.
Hohmann, H.P., et al., 1990. Tumor necrosis factors-alpha and -beta bind to the same two types of tumor necrosis factor receptors and maximally activate the transcription factor NF-kappa B at low receptor occupancy and within minutes after receptor binding. J. Biol. Chem. 265, 15183–15188.
Hoozemans, J.J., et al., 2006. Neuroinflammation and regeneration in the early stages of Alzheimer's disease pathology. Int. J. Dev. Neurosci. 24, 157–165.
Jakobsson, J., Lundberg, C., 2006. Lentiviral vectors for use in the central nervous system. Molec. Ther. 13, 484–493.
Janelsins, M.C., et al., 2005. Early correlation of microglial activation with enhanced tumor necrosis factor-alpha and monocyte chemoattractant protein-1 expression specifically within the entorhinal cortex of triple transgenic Alzheimer's disease mice. J. Neuroinflammation 2, 23.
Janelsins, M.C., et al., 2008. Chronic neuron-specific tumor necrosis factor-alpha expression enhances the local inflammatory environment ultimately leading to neuronal death in 3xTg-AD mice. Am. J. Pathol. 173, 1768–1782.
Kim, J., et al., 2007. Abeta40 inhibits amyloid deposition in vivo. J. Neurosci. 27, 627–633.
Kimberly, W.T., et al., 2005. Physiological regulation of the beta-amyloid precursor protein signaling domain by c-Jun N-terminal kinase JNK3 during neuronal differentiation. J. Neurosci. 25, 5533–5543.
Kitazawa, M., et al., 2005. Lipopolysaccharide-induced inflammation exacerbates tau pathology by a cyclin-dependent kinase 5-mediated pathway in a transgenic model of Alzheimer's disease. J. Neurosci. 25, 8843–8853.
Koenigsknecht-Talboo, J., Landreth, G.E., 2005. Microglial phagocytosis induced by fibrillar beta-amyloid and IgGs are differentially regulated by proinflammatory cytokines. J. Neurosci. 25, 8240–8249.
LaFerla, F.M., et al., 1997. Neuronal cell death in Alzheimer's disease correlates with apoE uptake and intracellular Abeta stabilization. J. Clin. Invest. 100, 310–320.
Lahiri, D.K., et al., 2003. Role of cytokines in the gene expression of amyloid beta-protein precursor: identification of a 5′-UTR-binding nuclear factor and its implications in Alzheimer's disease. J. Alzheimer's Dis. 5, 81–90.
Launer, L., 2003. Nonsteroidal anti-inflammatory drug use and the risk for Alzheimer's disease: dissecting the epidemiological evidence. Drugs 63, 731–739.
Lemere, C.A., et al., 1996. The E280A presenilin 1 Alzheimer mutation produces increased A beta 42 deposition and severe cerebellar pathology. Nat. Med. 2, 1146–1150.
Levites, Y., et al., 2006. Intracranial adeno-associated virus-mediated delivery of anti-pan amyloid beta, amyloid beta40, and amyloid beta42 single-chain variable fragments attenuates plaque pathology in amyloid precursor protein mice. J. Neurosci. 26, 11923–11928.
Lewis, J., et al., 2001. Enhanced neurofibrillary degeneration in transgenic mice expressing mutant tau and APP. Science 293, 1487–1491.
Liao, Y.F., et al., 2004. Tumor necrosis factor-alpha, interleukin-1beta, and interferon-gamma stimulate gamma-secretase-mediated cleavage of amyloid precursor protein through a JNK-dependent MAPK pathway. J. Biol. Chem. 279, 49523–49532.
Lopera, F., et al., 1997. Clinical features of early-onset Alzheimer disease in a large kindred with an E280A presenilin-1 mutation. JAMA 277, 793–799.
Ma, S.L., et al., 2004. Association between tumor necrosis factor-alpha promoter polymorphism and Alzheimer's disease. Neurology 62, 307–309.

Marchetti, L., et al., 2004. Tumor necrosis factor (TNF)-mediated neuroprotection against glutamate-induced excitotoxicity is enhanced by N-methyl-D-aspartate receptor activation. Essential role of a TNF receptor 2-mediated phosphatidylinositol 3-kinase-dependent NF-kappa B pathway. J. Biol. Chem. 279, 32869–32881.
McCoy, M.K., et al., 2006. Blocking soluble tumor necrosis factor signaling with dominant-negative tumor necrosis factor inhibitor attenuates loss of dopaminergic neurons in models of Parkinson's disease. J. Neurosci. 26, 9365–9375.
McGeer, P.L., et al., 1987. Reactive microglia in patients with senile dementia of the Alzheimer type are positive for the histocompatibility glycoprotein HLA-DR. Neurosci. Lett. 79, 195–200.
McGeer, E.G., McGeer, P.L., 2003. Inflammatory processes in Alzheimer's disease. Prog. Neuro-psychopharmacol. Biol. Psychiatry 27, 741–749.
McGeer, P.L., McGeer, E.G., 2007. NSAIDs and Alzheimer disease: epidemiological, animal model and clinical studies. Neurobiol. Aging 28, 639–647.
McPhie, D.L., et al., 1997. Neuronal expression of beta-amyloid precursor protein Alzheimer mutations causes intracellular accumulation of a C-terminal fragment containing both the amyloid beta and cytoplasmic domains. J. Biol. Chem. 272, 24743–24746.
Mrak, R.E., Griffin, W.S., 2005. Glia and their cytokines in progression of neurodegeneration. Neurobiol. Aging 26, 349–354.
Nee, L.E., et al., 1983. A family with histologically confirmed Alzheimer's disease. Arch. Neurol. 40, 203–208.
Oddo, S., et al., 2003a. Amyloid deposition precedes tangle formation in a triple transgenic model of Alzheimer's disease. Neurobiol. Aging 24, 1063–1070.
Oddo, S., et al., 2003b. Triple-transgenic model of Alzheimer's disease with plaques and tangles: intracellular Abeta and synaptic dysfunction. Neuron 39, 409–421.
Ohno, M., et al., 2007. BACE1 gene deletion prevents neuron loss and memory deficits in 5XFAD APP/PS1 transgenic mice. Neurobiol. Dis. 26, 134–145.
Oster-Granite, M.L., et al., 1996. Age-dependent neuronal and synaptic degeneration in mice transgenic for the C terminus of the amyloid precursor protein. J. Neurosci. 16, 6732–6741.
Paganelli, R., et al., 2002. Proinflammatory cytokines in sera of elderly patients with dementia: levels in vascular injury are higher than those of mild-moderate Alzheimer's disease patients. Exp. Gerontol. 37, 257–263.
Paxinos, G., Franklin, K.B.J., 2001. The Mouse Brain in Stereotaxic Coordinates. Academic Press, San Diego, CA.
Pfeifer, A., et al., 2002. Transgenesis by lentiviral vectors: lack of gene silencing in mammalian embryonic stem cells and preimplantation embryos. Proc. Natl. Acad. Sci. U. S. A. 99, 2140–2145.
Qiao, X., et al., 2001. Neuroinflammation-induced acceleration of amyloid deposition in the APPV717F transgenic mouse. Eur. J. Neurosci. 14, 474–482.
Saura, J., et al., 2003. High-yield isolation of murine microglia by mild trypsinization. Glia 44, 183–189.
Scheinfeld, N., 2004. A comprehensive review and evaluation of the side effects of the tumor necrosis factor alpha blockers etanercept, infliximab and adalimumab. J. Derm. Treat. 15, 280–294.
Sheng, J.G., et al., 2003. Lipopolysaccharide-induced-neuroinflammation increases intracellular accumulation of amyloid precursor protein and amyloid beta peptide in APPswe transgenic mice. Neurobiol. Dis. 14, 133–145.
Sinha, S., Lieberburg, I., 1999. Cellular mechanisms of beta-amyloid production and secretion. Proc. Natl. Acad. Sci. U. S. A. 96, 11049–11053.
Steed, P.M., et al., 2003. Inactivation of TNF signaling by rationally designed dominant-negative TNF variants. Science 301, 1895–1898.
Tan, Z.S., et al., 2007. Inflammatory markers and the risk of Alzheimer disease: the Framingham Study. Neurology 68, 1902–1908.
Taylor, L., et al., 2006. Neurotrophin-3 gradients established by lentiviral gene delivery promote short-distance axonal bridging beyond cellular grafts in the injured spinal cord. J. Neurosci. 26, 9713–9721.
Tobinick, E., et al., 2006. TNF-alpha modulation for treatment of Alzheimer's disease: a 6-month pilot study. Med. Gen. Med. 8, 25.
Valasek, M.A., Repa, J.J., 2005. The power of real-time PCR. Adv. Physiol. Educ. 29, 151–159.
van Gool, W.A., et al., 2003. Anti-inflammatory therapy in Alzheimer's disease: is hope still alive? J. Neurol. 250, 788–792.
Whalen, B.M., et al., 2005. Small non-fibrillar assemblies of amyloid beta-protein bearing the Arctic mutation induce rapid neuritic degeneration. Neurobiol. Dis. 20, 254–266.
Wyss-Coray, T., Mucke, L., 2002. Inflammation in neurodegenerative disease—a double-edged sword. Neuron 35, 419–432.
Yamamoto, M., et al., 2007. Interferon-gamma and tumor necrosis factor-alpha regulate amyloid-beta plaque deposition and beta-secretase expression in Swedish mutant APP transgenic mice. Am. J. Pathol. 170, 680–692.
Yankner, B.A., et al., 1989. Neurotoxicity of a fragment of the amyloid precursor associated with Alzheimer's disease. Science 245, 417–420.
Zalevsky, J., et al., 2007. Dominant-negative inhibitors of soluble TNF attenuate experimental arthritis without suppressing innate immunity to infection. J. Immunol. 179, 1872–1883.
Zhao, J., et al., 2007. Beta-site amyloid precursor protein cleaving enzyme 1 levels become elevated in neurons around amyloid plaques: implications for Alzheimer's disease pathogenesis. J. Neurosci. 27, 3639–3649.